Synthesis, experimental evaluation and molecular modelling of hydroxamate derivatives as zinc metalloproteinase inhibitors

Stian Sjøli[a], Elisa Nuti[b], Caterina Camodeca[c], Irina Bilto[d], Armando Rossello[b], Jan-Olof Winberg[a], Ingebrigt Sylte[a*] and Olayiwola A. Adekoya[d]

[a]Department of Medical Biology, Faculty of Health Sciences, UiT The Arctic University of Norway, NO-9037 Tromsø, Norway.
[b]Dipartimento di Farmacia, Università di Pisa, Via Bonanno 6, 56126 Pisa, Italy.
[c]Division of Immunology, Transplants and Infectious Diseases, San Raffaele Scientific Institute, Milan, Italy
[d]Department of Pharmacy, Faculty of Health Sciences, UiT The Arctic University of Norway, NO-9037 Tromsø, Norway.

* Corresponding author:

Ingebrigt Sylte, Department of Medical Biology, Faculty of Health Sciences, University of Tromsø, NO-9037 Tromsø, Norway
Email: Ingebrigt.Sylte@uit.no
Tel :+47 77644705

Abstract

Enzymes of the M4 family of zinc-metalloproteinases are virulence factors secreted from gram-positive or gram-negative bacteria, and putative drug targets in the treatment of bacterial infections. In order to have a therapeutic value such inhibitors should not interfere with endogenous zinc-metalloproteinases. In the present study we have synthesised a series of hydroxamate derivatives and validated the compounds as inhibitors of the M4 enzymes thermolysin and pseudolysin, and the endogenous metalloproteinases ADAM-17, MMP-2 and MMP-9 using experimental binding studies and molecular modelling. In general, the compounds are stronger inhibitors of the MMPs than of the M4 enzymes, however, an interesting exception is LM2. The compounds bound stronger to pseudolysin than to thermolysin, and the molecular modelling studies showed that occupation of the S_2' subpocket by an aromatic group is favourable for strong interactions with pseudolysin.

Keywords: zinc-metalloproteinases, M4 family, bacterial virulence factors, Matrix metalloproteinases, Adamalysins, enzyme selective inhibition, docking and scoring, molecular dynamics simulations

.

1. Introduction

The discovery and approval of new antibacterial drugs has stagnated, and it is an urgent need to develop new effective strategies against bacterial infections with a low risk for resistance development. Selective inhibitors weakening the pathogen without directly targeting its viability is a promising strategy since the pathogen will have reduced capacity to suppress or avoid the host immune system [1]. Such inhibitors can be used as adjuvants to reduce the concentration of antibiotics, and thereby reduce the risk of resistance development. Thermolysin and pseudolysin belong to the M4 family of metalloproteinases (http://merops.sanger.ac.uk). Most of the M4 family members are virulence factors secreted from gram-positive or gram-negative bacteria [2, 3]. These enzymes degrade extracellular proteins and peptides that the bacteria uses for nutrition prior to sporulation. The family includes enzymes from pathogens such as *Legionella, Listeeria, Clostridium, Staphylococcus, Pseudomonas* and *Vibrio*, and are important contributors in various bacterial infections [4]. Inhibitors of pseudolysin and thermolysin may weaken the pathogen and be a putative strategy in the fight against bacterial infections [5-9]. In order to have therapeutic potentials, bacterial M4 enzyme inhibitors should not interfere with the substrate degradation of endogenous zinc metalloproteinases of the infected host, like the matrix metalloproteinases (MMPs) and the adamalysins (ADAMs).

Thermolysin from *Bacillus B. thermoproteolyticus* was the first enzyme of the M4 family to be sequenced and to have the three-dimensional (3D) structure determined, and the family was also named the thermolysin family of metalloproteinases. The X-ray crystal structures of the M4 family members show that the enzymes contain a catalytic zinc ion coordinated by three amino acids and a water molecule [10]. However, they have structural similarities with endogenous zinc metalloproteinases in the region of the catalytic site [4, 11]. Obtaining appropriate specificity is therefore problematic in the development of compounds targeting M4

zinc metalloproteinases. Both peptidic and non-peptidic molecules have been identified as thermolysin [12-14] and pseudolysin [15, 16] inhibitors, and so far all published compounds target the catalytic zinc. However, an exhaustive study able to lead to the discovery of nanomolar and selective thermolysin or pseudolysin non-peptidic inhibitors is still missing. The crystal structures complexes with small molecules show that upon binding, the zinc coordinating water molecule is replaced by one or two oxygen atoms from the inhibitor forming a monodentate or bidentate arrangements with the catalytic zinc ion [17-19]. The X-ray complexes also show that the overall geometry of the binding pocket can be divided into three subpockets, the S_1'-, S_2'-, and S_1-subpockets [4, 20]. The S_1'-subpocket is the main binding region for substrate recognition, and accommodates specifically hydrophobic amino acids of the substrate, both for thermolysin and pseudolysin. The S_2' – subpocket is also quite hydrophobic, while the S_1 – subpocket is larger and more hydrophilic than the other two subpockets.

In an effort to develop selective thermolysin and pseudolysin inhibitors able to spare the human MMPs and ADAMs, we have, in the present study used compounds belonging to our in-house library of MMP inhibitors. Some new or already published compounds, with a low affinity against MMPs (in the micromolar range) were chosen and screened against thermolysin and pseudolysin, while some nanomolar MMP-2 inhibitors were selected as reference compounds. The series of compounds used in the present study are hydroxamates belonging to several chemical classes, all derived from a common general structure: secondary and tertiary arylsulfonamides, arylamides, biarylsulfones, *N*-benzyloxy aminoacid hydroxamates (Fig. 1). Such a chemical diversity could be useful to identify the structural characteristics necessary to have a strong binding to thermolysin and pseudolysin catalytic sites. Hydroxamates were chosen because they are known to have a strong zinc-chelating effect. The compounds were

also evaluated by molecular modelling in order to assess the binding mode to the tested zinc metalloproteinases.

2. Results

2.1 Chemistry

The compounds **ARP101**, **EN178**, **LM2** and **FC19** were synthesised as previously reported [21-24]. Compound **EN204** was prepared as described in Scheme 1. Sulfonamide **1** [25] was alkylated by treatment with 1-iodo-2-methylpropane in DMF using potassium carbonate as base. Subsequently, *N*-isobutyl derivative **2** was submitted to acid hydrolysis to give carboxylate **3** which was finally converted into the corresponding hydroxamate **EN204** by condensation with *O*-(*tert*-butyldimethylsilyl)hydroxylamine and acid cleavage by trifluoroacetic acid (TFA).

Scheme 1. Synthesis of compound **EN204**

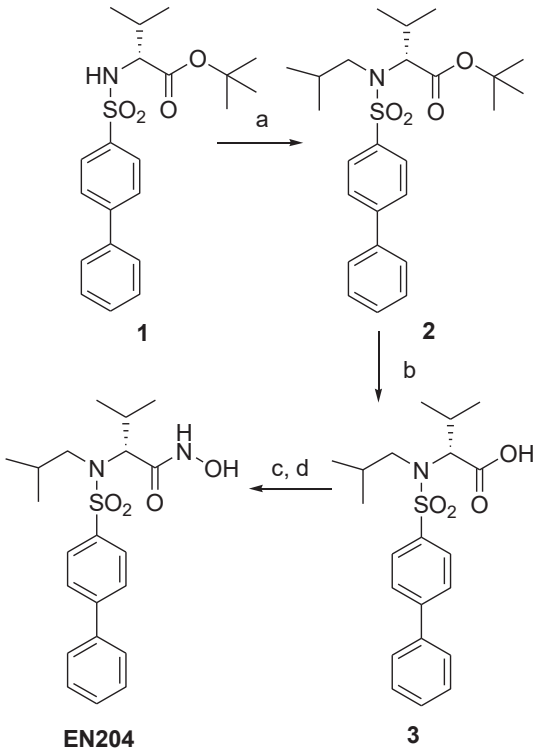

[a] Reagents and conditions: (a) K_2CO_3, isobutyl iodide, DMF; (b) TFA, CH_2Cl_2, 0 °C; (c) $TBDMSiONH_2$, EDC, CH_2Cl_2; (d) TFA, CH_2Cl_2, 0 °C.

Compound **FO9** was synthesised as described in Scheme 2. Biphenyl-4-sulfonyl chloride was added to 3-aminopropanoic acid in water and dioxane using triethylamine (TEA) as base. Carboxylate **4** was then condensed with *O*-(*tert*-butyldimethylsilyl)hydroxylamine in the presence of 1-[3-(dimethylamino)propyl]-3-ethyl carbodiimide hydrochloride (EDC) to give silyl intermediate **5** which afforded hydroxamate **FO9** after acid cleavage with TFA.

Scheme 2. Synthesis of compound **FO9**

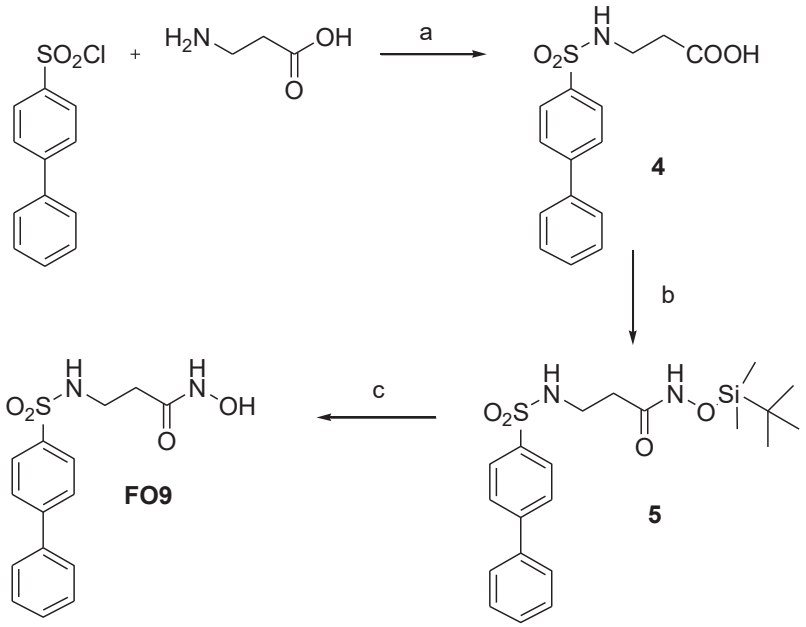

[a] Reagents and conditions: (a) TEA, H_2O, dioxane; (b) $TBDMSiONH_2$, EDC, CH_2Cl_2; (d) TFA, CH_2Cl_2, 0 °C.

Compound **FC31** was synthesised as reported in Scheme 3. *tert*-Butyl ester **7** was prepared by esterification of carboxylic acid **6** [24] with *N,N*-dimethylformamide di-*tert*-butyl acetal in

toluene. The phenolic group of compound **7** was alkylated by treatment with 2-(3-bromopropyl)isoindoline-1,3-dione in acetone using potassium carbonate as base to give **8**. Ester **8** was oxidized to the corresponding sulfone **9** using Oxone in methanol/THF/H_2O, and subsequently hydrolyzed to the corresponding carboxylic acid **10** by treatment with TFA. Carboxylate **10** was finally converted into the corresponding hydroxamate **FC31** by condensation with *O*-(*tert*-butyldimethylsilyl)hydroxylamine and acid cleavage by TFA.

Scheme 3. Synthesis of compound **FC31**

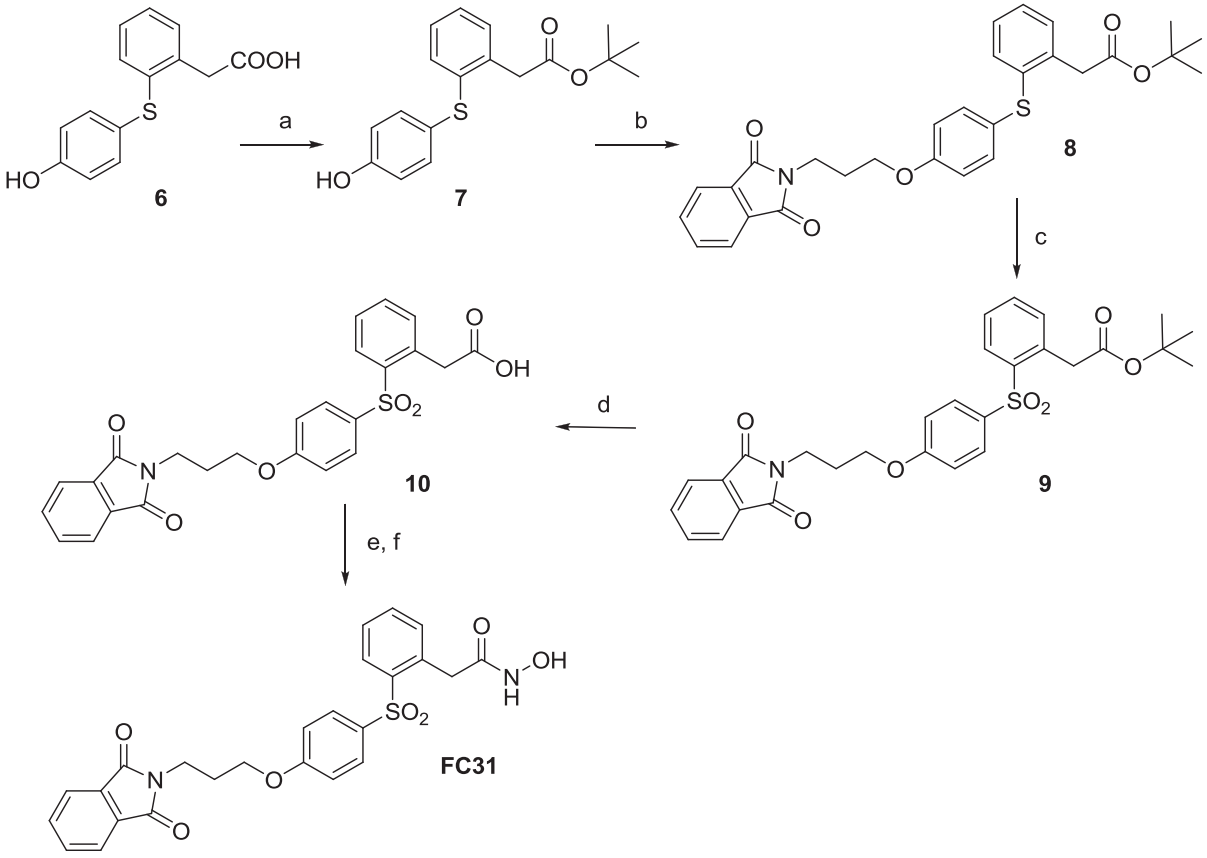

[a] Reagents and conditions: (a) $(CH_3)_2NCH[OC(CH_3)_3]_2$, toluene, 95ºC; (b) K_2CO_3, 2-(3-bromopropyl)isoindoline-1,3-dione, acetone, reflux; (c) Oxone, MeOH, THF, H_2O; (d) TFA, CH_2Cl_2, 0 °C; (e) $TBDMSiONH_2$, EDC, CH_2Cl_2; (f) TFA, CH_2Cl_2, 0 °C.

Compound **ML25** was synthesised as reported in Scheme 4. Carboxylic acid **12** was prepared by acid hydrolysis of the previously described *tert*-butyl ester **11** [26]. The corresponding hydroxamic acid **ML25** was obtained by condensation of **12** with *O*-(*tert*-butyldimethylsilyl)hydroxylamine followed by acid cleavage with TFA.

Scheme 4. Synthesis of compound **ML25**

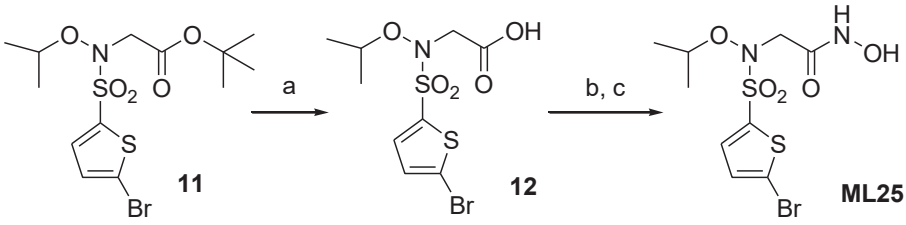

[a] Reagents and conditions: (a) TFA, CH_2Cl_2, 0 °C; (b) $TBDMSiONH_2$, EDC, CH_2Cl_2; (c) TFA, CH_2Cl_2, 0 °C.

Compound **EN181** was prepared as reported in Scheme 5. Commercially available 4-phenoxybenzoic acid was reacted with *O*-isopropylhydroxylamine hydrochloride in the presence of *N*-methylmorpholine (NMM) and EDC in CH_2Cl_2 to give the isopropoxyamide **13**. A Mitsunobu reaction of **13** with the alcohol **14** [27] in the presence of diisopropyl azodicarboxylate (DIAD) and triphenylphosphine gave the *tert*-butyl ester **15** which was converted to its corresponding carboxylate **16** by acid hydrolysis with TFA. Hydroxamic acid **EN181** was finally obtained by condensation of **16** with *O*-(*tert*-butyldimethylsilyl)hydroxylamine followed by acid cleavage with TFA.

Scheme 5. Synthesis of compound **EN181**

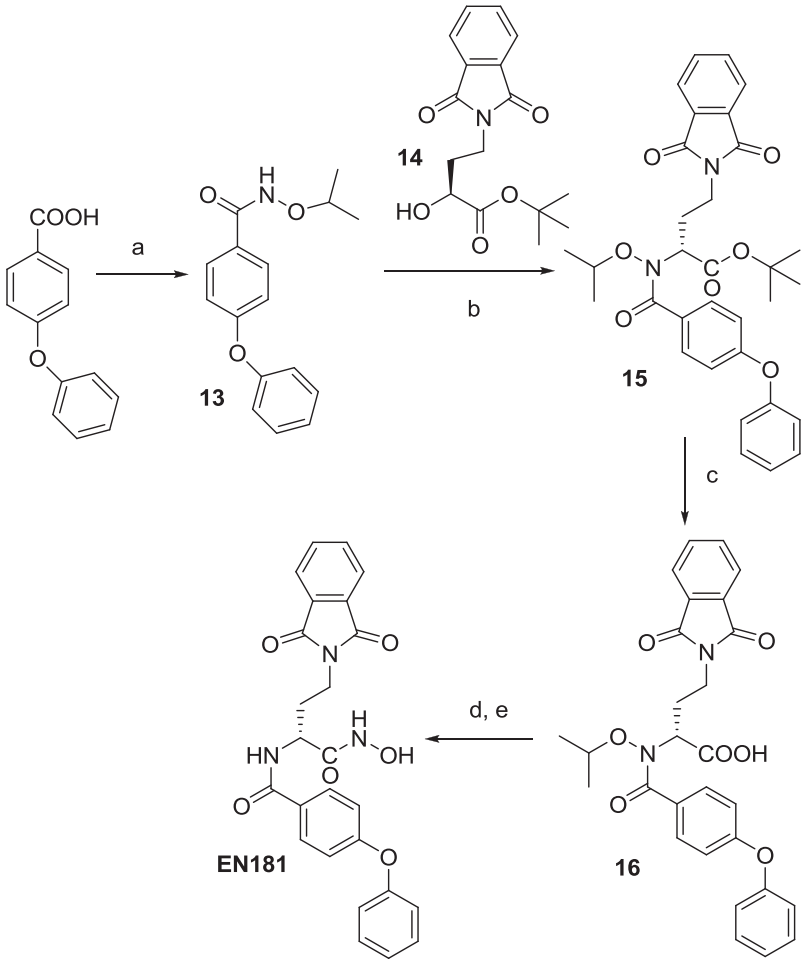

[a] Reagents and conditions: (a) *O*-isopropyl hydroxylamine HCl, NMM, EDC, CH_2Cl_2; (b) PPh_3, DIAD, THF; (c) TFA, CH_2Cl_2, 0 °C; (d) $TBDMSiONH_2$, EDC, CH_2Cl_2; (e) TFA, CH_2Cl_2, 0 °C;

Compound **CC30** was prepared as reported in Scheme 6. Commercially available 4-methoxybenzene-1-sulfonyl chloride was reacted with *O*-(1-adamantyl)oxyamine **17** in THF, yielding sulfonamide **18**, which was alkylated with *tert*-butyl bromoacetate to give ester **19**. Acid hydrolysis of ester **19** afforded carboxylate **20**, which was finally converted to its corresponding hydroxamate by condensation with *O*-(*tert*-butyldimethylsilyl)hydroxylamine and acid cleavage by TFA.

Scheme 6. Synthesis of compound **CC30**

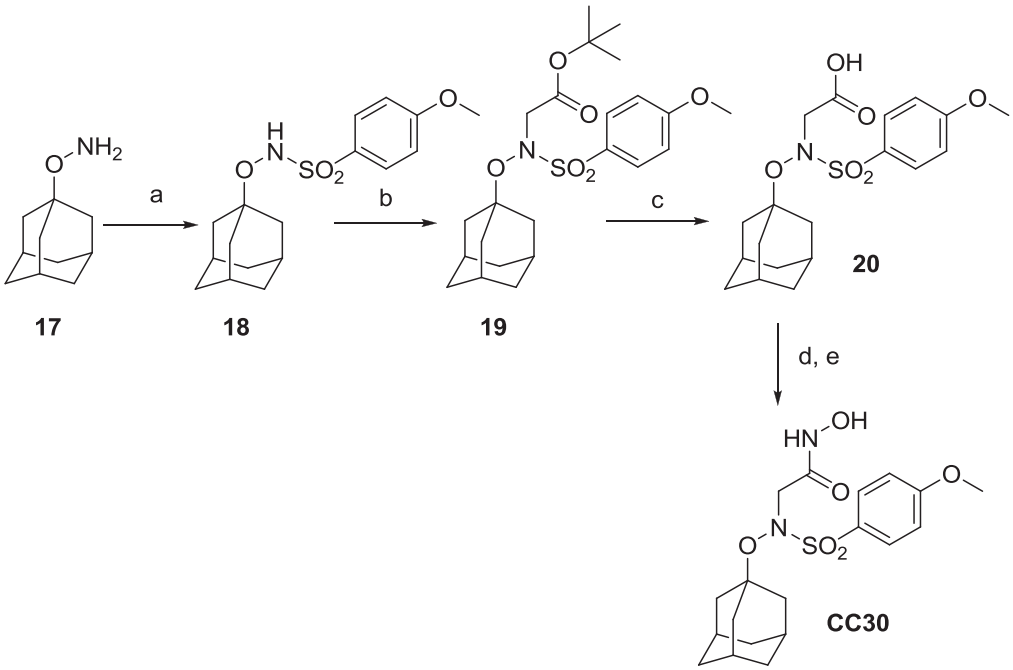

[a] Reagents and conditions: (a) 4-methoxybenzene-1-sulfonyl chloride, NMM, THF; (b) $BrCH_2COO$*t*-Bu, Cs_2CO_3, Bu_4NHSO_4, DMF; (c) TFA, CH_2Cl_2, 0°C; (d) $TBDMSiONH_2$, EDC, CH_2Cl_2; (e) TFA, CH_2Cl_2, 0°C.

2.2. Determination of K_m for thermolysin and pseudolysin

During the conditions used, K_m values for the fluorogenic Abz-Ala-Gly-Leu-Ala-p-nitrobenzylamide (AGLA) substrate with thermolysin and pseudolysin were 68 ± 10 and 128 ± 23 μM, respectively, while the corresponding values for the fluorogenic substrate Mca-Arg-Pro-Pro-Gly-Phe-Ser-Ala-Phe-Lys-(Dnp)-OH -(Bradykinin-like substrate; BLS) were 15 ± 3 and 10 ± 3 μM. With the AGLA substrate this resulted in [S]/Km values of 0.22 for thermolysin and 0.08 for pseudolysin, while the corresponding values for BLS were 0.11 and 0.17. The relation between K_i and IC_{50} for a substrate competitive inhibitor is $K_i = IC_{50} / (1+[S]/K_m)$. Thus the obtained IC_{50} values for the two enzymes with the two different substrates will reflect the dissociation constant K_i.

2.3. Enzyme inhibition studies

IC_{50} values of the compounds were measured *in vitro* both for thermolysin and pseudolysin using the fluorogenic substrates AGLA and BLS. The new hydroxamates EN204, FO9, FC31, EN181, ML25 and CC30 were also tested *in vitro* for their ability to inhibit human recombinant MMP-2 and MMP-9 by a fluorometric assay, with the fluorogenic peptide Mca-Lys-Pro-Leu-Gly-Leu-Dap(Dnp)-Ala-Arg-NH_2 (FS-6) [28] as the substrate. MMP-2, MMP-9, and ADAM-17 were chosen among the 23 human MMPs and 21 human ADAMs as prototype enzymes to test the selectivity of the new compounds. The compounds ARP101 [21, 26], EN178 [22], FC19 [24] and LM2 [23] have previously been tested for inhibition of different MMPs including MMP-2 and MMP-9. The IC_{50} values are shown in Table 1.

In general, the compounds exhibit a stronger inhibition of the MMPs than of the bacterial M4 enzymes and ADAM-17 (Table 1). In particular, ARP101, EN178, EN204 which inhibit MMP-2 and MMP-9 in the nM range. The benzyloxy aminoacid hydroxamate LM2 is the only compound that shows a stronger inhibition of pseudolysin and thermolysin than of MMP-2, MMP-9 and ADAM-17 (Table 1). In fact, the inhibitory activities (IC_{50} values) of LM2 toward the M4 enzymes are in the range of 1.1- 9.5 μM while the IC_{50} values toward MMP-2, MMP-9 and ADAM-17 are 34, 81 and 100 μM, respectively.

In general, the IC_{50} values also indicated that the compounds bound stronger to pseudolysin than to thermolysin (Table 1). Several compounds such as LM2, ML25, EN181, FC19 and FC31 have a good binding affinity to pseudolysin, with IC_{50} values in the lower μM region. The best binders for both pseudolysin and thermolysin are LM2 and ML25 (Table 1). For pseudolysin, LM2 has an IC_{50} value of 1 to 2 μM (depending on the substrate used for the assay). For thermolysin, LM2 has an IC_{50} value of 9.5 μM. ML25 also binds quite strongly both to thermolysin and pseudolysin, with IC_{50} values in the range of 3-33 μM.

2.4 Molecular modelling

Molecular modelling studies were performed to study the binding modes of the compounds for the bacterial M4 enzymes, MMP-2 and MMP-9 and if possibly obtain structural insight into selective pseudolysin and thermolysin inhibition based on the *in vitro* enzymatic assays. All compounds were docked into the four enzyme structures. However, in particular three ligands are described in detail: LM2 (more active for M4 enzymes than for MMPs), FO9 (similar activity both for pseudolysin and MMP-9), and ARP101 (more active for MMPs than for M4 enzymes). The Pseudolysin-inhibitor complexes after docking were also structurally refined by molecular dynamics (MD) simulations.

Docking into pseudolysin, MMP-2 and MMP-9 were performed with the ICM program [29]. Initial docking into thermolysin was performed with the Glide program of the Schrødinger program package [30]. However, the Glide docking could not give any clear prediction about the binding mode of the inhibitors in thermolysin and the inhibitors were therefore re-docked in thermolysin with the ICM software. Docked complexes were evaluated based on scoring and similarities with complexes present in the PDB-database.

The complexes of ARP101, FO9 and LM2 with pseudolysin and thermolysin after docking are shown in Fig. 2. Docking of LM2 into pseudolysin (Fig. 2) indicated that the hydroxamate part formed bidentate interaction with the zinc atom, while the ring system occupied the S_2'-subpocket and the aliphatic butane chain pointed in the direction of the S_1'-subpocket (Fig. 2). The oxygen atoms of the hydroxamate CO and OH groups interact with the zinc, while the hydrogen atom of the OH-groups interacts with the side chain of Glu141, and the hydroxamate NH forms a hydrogen bond with the backbone of Tyr114, and also interacts with His140. After docking, ML25 and FO9 had quite similar orientation as LM2 with the ring system occupying the S_2'-subpocket (Fig. 2), however, for FO9 binding poses with the ring system within the S_1-subpocket were also observed. Docking of ARP101, EN178, EN204 and FC19 indicated that the aromatic ring system of these compounds occupy the S_1-subpocket of pseudolysin. The

hydroxamate NH-group of ARP101 formed a hydrogen bond with the backbone of Ala113, while the hydroxamate OH-group formed a hydrogen bond with Glu141 (Fig.2).

In thermolysin clear prediction of their binding poses was not obtained neither with Glide nor ICM. Both Glide and ICM docking showed docking poses for the strongest thermolysin binders LM2 and ML25 with their ring systems occupying both the S_2'- and the S_1-subpocket, and based on the docking we could not rank one of the predicted orientations in front of the other. In both orientations LM2 and ML25 formed a bidentate interaction with the zinc. Fig. 2 shows LM2 in a pose with the ring system in the S_1-subpocket of thermolysin interacting with Phe114 (displayed in Fig. 2) and Asp116. In that orientation the hydroxamate CO-groups form hydrogen bonds with the side chain of Arg203, while the NH-group interacts with Glu143 (Fig. 2).

Several X-ray complexes of thermolysin with small molecules are available in the PDB-database, while quite few are available for pseudolysin. Evaluating the docking poses based on known X-ray complexes is therefore easier for thermolysin than for pseudolysin. The structural stability of the pseudolysin-inhibitor complexes was therefore tested by 24 ns of molecular dynamics (MD) simulations. The MD simulations indicated that pseudolysin – inhibitor complexes were stable during 24 ns of MD simulations, and the main interactions were similar before and after 24 ns of MD. Amino acids within 4 Å of the inhibitors after MD are shown in Table 2.

Docking of the compounds in MMPs indicated that the compounds interact quite similarly in both MMP-2 and MMP-9, with the ring system in the S_1'-subpocket and with a bidentate interaction between the hydroxamate groups of the compound and the zinc. The complexes of MMP-9 with ARP101, FO9 and LM2 are shown in Fig. 3. In MMP-9 the ring system of the high affinity binder ARP101 (Table 1) occupy the S_1'-subpocket in between Leu397, Val398, His401, Leu418, and Tyr423. The SO_2 group interacts with the backbone of

Leu187 and Ala189, the hydroxamate NH-group forms a hydrogen bond with the backbone of Ala189, the hydroxamate CO-group coordinates the zinc, while the OH-group coordinates the zinc and forms a hydrogen bond with Glu402. One of isopropyl groups of ARP101 interacts in the S_2'-subpocket (Fig. 3). LM2 which is a much weaker MMP-2 and MMP-9 binder than ARP101 coordinates the zinc in the same way as ARP101, however, in contrast to ARP101 the hydroxamate OH-group did not form a hydrogen bond with the enzyme, and the structure did not penetrate deeply into the S_1'- and S_2'- subpocket as did ARP101.

3. Discussion

A series of hydroxamate derivatives (Fig. 1) were synthesised and tested for their binding affinity to pseudolysin, thermolysin, MMP-2, MMP-9 and ADAM-17 by *in vitro* binding studies (Table 1). Molecular modelling studies were also performed with the compounds interacting with thermolysin, pseudolysin, MMP-2 and MMP-9. Our studies showed that most of the compounds bound much stronger to MMP-2 and MMP-9 than to the bacterial M4 enzymes and ADAM-17 (Table 1). The only exception was LM2 that bound stronger to pseudolysin and thermolysin than to the human zinc metalloproteinases.

The average complexes after docking and MD of pseudolysin with ML25 indicated that the hydroxamate part formed bidentate interactions with the zinc atom, while the 2-bromothiophene group occupied the S_2'-subpocket. LM2 had a similar orientation in pseudolysin with the ring system occupying the S_2'-subpocket (Fig. 2). This orientation gave strong interactions with amino acids in the S_2'-subpocket. Energy decomposition of the ML25-psedolysin interactions using the Analyze module of the AMBER package [31] showed that ML25 had interaction energies of – 6.4 kcal/mol with Ala 113, while the interactions with Leu197 and Arg198 in the S_2'-subpocket were -3.8 kcal/mol and -3.5 kcal/mol, respectively.

Strong interaction with amino acids in the S_2'-subpocket seems to be the main reason for that ML25 and LM2 are moderately strong pseudolysin binders.

The X-ray crystal structure of pseudolysin and thermolysin in complex with inhibitors were used as guides for evaluating the docking poses of the various inhibitors. Fewer experimentally complexes are available for pseudolysin than for thermolysin, but MD simulations for 24 ns showed that the obtained pseudolysin-ligand complexes were structurally stable. The interaction of LM2 with pseudolysin is also similar to that seen in X-ray structure complex (PDB id: 1u4g and 3dbk). The superimposition of the best poses from the docking experiments with LM2 almost replicated the pose of the inhibitor (N-(1-carboxy-3-phenylpropyl) phenylalanyl-alpha-asparagine) in the X-ray crystal structure with pseudolysin. Amino acids within 4 Å of LM2 after MD are shown in Table 2. The two X-ray derived structures of pseudolysin in complex with small molecule inhibitors (1u4g and 3dbk) show that the inhibitors interact with Asn112, Ala113, Glu141, Arg198 and are deeply placed in the pocket consisting of Leu132 (S_1'), Val137 (S_1'), Ile186 (S_2'), Leu197 (S_2'), and F129 (S_2'). The docking and MD simulations therefore indicate that the strongest pseudolysin binder in the present study interacts with pseudolysin within a binding mode similar to that seen in the known X-ray crystal structure complexes 1u4g and 3dbk (Table 2).

All the ligands with butyl-side chains (ARP101, EN178 and EN204) had weak binding affinities for pseudolysin and thermolysin, and EN178 had the weakest pseudolysin binding of all studied compounds (Table 1). The docking poses of EN178, ARP101 and EN204 showed a lack of the important interactions within S_2'-subpocket as observed for LM2, and in the X-ray complexes of inhibitors with pseudolysin. The complex of ARP101 with pseudolysin is shown in Fig. 2. In contrast to the strongest pseudolysin binder LM2, the aromatic ring systems of ARP101, EN178, EN204, FO9 (for most of the poses) and FC19 all occupied the S_1-subpocket of pseudolysin after docking and MD. The hydroxamate group formed bidentate interactions

with the Zinc atom. The average structures after MD indicated that FC31 interacted with pseudolysin in a bent conformation with the phthalimide ring system in the S_1-subpocket, and the other ring system partly in the S_2'-subpocket and partly outside the three subpockets of pseudolysin. FC31 also bound quite strongly to pseudolysin (Table 1). After MD with EN181, the diphenyl ether group interacted in the S_1-subpocket, while the phthalimide group interacted in the S_2'-subpocket but also had interactions outside the subpockets of pseudolysin.

X-ray structure complexes with thermolysin show that the S_1-subpocket can accommodate hydrophobic ligand parts, while S_1' and S_2'-subpockets can host quite similar groups and that hydrophobic residues of peptides are favoured. However, the S_2'-subpocket is more easily accessible for water molecules than the S_1-subpocket [32]. Docking LM2 and ML25 into thermolysin showed docking poses both with the aromatic ring system in the S_2'- and the S_1-subpocket, and we could not rank the poses relative to each other based on scoring. In an X-ray complex from the PDB-database (PDB code 1pe5) the inhibitor interacts within the S_1'- and S_2'-subpockets and not in the S_1-subpocket, while other X-ray thermolysin complexes with small molecular inhibitors also show that the inhibitor may occupy the S_1-subsite as well. In the docking poses with the aromatic ring of LM2 in the S_1-subpocket, the aromatic ring interacts with Phe114, Trp115, Tyr157 and His146. The docking of LM2 and ML25 indicated that both orientations could be possible in thermolysin. As noted previously there are subtle differences between the active site of pseudolysin and thermolysin [33]. The S_2' -subpocket of pseudolysin is bigger than that of thermolysin, and the aromatic ring system of LM2 and ML25 seem to obtain stable interactions with the S_2' subpocket in pseudolysin and contribute to relative stable pseudolysin-inhibitor complexes.

Docking into the M4 enzymes showed that amino acids within the S_1- and S_2'-subpockets are important for binding. As discussed in a recent paper, there are structural differences between the M4 enzymes and the MMPs in the region of these subpockets [33]. In MMP-2

and MMP-9, Leu83 and Tyr142 (MMP-2 numbering in the structure used for docking, the fibronectin-domain is replaced by a short peptide linker) are protruding into the binding pocket and contribute to a quite narrow access both to the S_1'- and S_2'-subpockets. These residues correspond to Leu188 and Tyr423 (Fig. 3) in the MMP-9 structure. The X-ray complex of a hydroxamate inhibitor with MMP-2 (PDB code 1hov) show that the inhibitor is able to tunnel in between Leu83 and Tyr142 and interact deeply in a binding pocket that includes Leu83, Ala84, Ala136, Leu137, Ala139, Ile141, Thr143, Pro148 and Arg148. These amino acids are both from the S_1'- and S_2'-subpockets. Docking of LM2, the worst MMP-2 and MMP-9 binder, but the best M4 binder, indicated that LM2 is not able to interact deeply within the S_1'- and S_2'-subpockets of MMP-9 (Fig. 3) and MMP-2, as observed in for the ligand in the 1hov complex of MMP-2. Investigating the top docked poses of ARP101 and EN204 (the inhibitors with lowest IC_{50} values with MMP-2) in MMP-2 showed that they are able to tunnel into the deep pocket similarly to that observed in 1hov X-ray structure and are not hindered by Leu83 and Tyr142 in MMP-2, and by Leu188 and Tyr423 in MMP-9. They are also able to form most of the interactions described above and interact close to the active site Zinc ion as seen in the 1hov structure. ARP101 forms hydrogen bonding interactions with Leu83 and Ala84 and with amino acids in the S_2'-subpocket and the deep S_1'-subpocket of MMP-2 and MMP-9.

4. Conclusions

Inhibitors targeting bacterial virulence factors such as the M4 zinc metalloproteinases has been suggested to be a novel strategy in the development of new antibacterial drugs [34]. However, zinc metalloproteinase inhibitors of therapeutic value should not interfere with the substrate degradation of endogenous zinc metalloproteinases of the infected host. In the present study we have synthesised and evaluated a series of hydroxamate derivatives (Fig. 1) as putative thermolysin and pseudolysin inhibitors. Some of these compounds (ARP101, EN178, LM2 and

FC19) have previously been reported as MMP inhibitors. Knowledge about structural determinants giving high affinity for the bacterial M4 zinc metalloproteinases but low affinity to human metalloproteinases like the MMPs is important for designing M4 inhibitors of therapeutic value in bacterial infections. Low MMP affinity may be important for avoiding the serious adverse effects including hepatotoxicity as observed for marimastat and other MMP inhibitors. The experimental testing and molecular modelling indicated that the aromatic group of the strongest binders (LM2 and ML25) binds to amino acids within the S_2'-subpocket of the M4 enzymes. For the other compounds with one aromatic group, the aromatic group is bigger, and occupied the S_1-subpocket of pseudolysin.

In general the compounds bound stronger to pseudolysin than to thermolysin. LM2 which binds stronger to thermolysin and pseudolysin than to MMP-2, MMP-9 and ADAM-17 provides, a good starting point for further hit evolution for a tailored lead design. Compounds that not penetrate deeply into a pocket consisting of amino acids within the S_1'- and S_2'-subpockets of the MMPs, but bind strongly within the S_2'-subpocket of the M4 enzymes may increase the affinity for M4 and decrease the affinity for MMP-2 and MMP-9.

5. Experimental section

5.1 Chemistry

Melting points were determined on a Kofler hotstage apparatus and are uncorrected. ^{1}H spectra were determined with a Varian Gemini 200 MHz spectrometer. Chemical shifts (δ) are reported in parts per million downfield from tetramethylsilane and referenced from solvent references. Coupling constants *J* are reported in hertz. The following abbreviations are used: singlet (s), doublet (d), triplet (t), double-doublet (dd), broad (br) and multiplet (m). Chromatographic separation was performed on silica gel columns by flash column chromatography (Kieselgel 40, 0.040–0.063 mm; Merck) or using ISOLUTE Flash Si II cartridges (Biotage). The reactions

were followed by thin-layer chromatography (TLC) on Merck aluminum silica gel (60 F254) sheets that were visualized under a UV lamp and hydroxamic acids were visualized with $FeCl_3$ aqueous solution. Evaporation was performed *in vacuo* (rotating evaporator). Sodium sulfate was always used as the drying agent. Commercially available chemicals were purchased from Sigma-Aldrich. Compounds ARP101, EN178, LM2 and FC19 have been synthesised as previously described [21-24].

(*R*)-*tert*-Butyl 2-(*N*-isobutylbiphenyl-4-ylsulfonamido)-3-methylbutanoate (2). To a solution of sulfonamide **1** (800 mg, 2.0 mmol) in DMF (32 mL) is added 1-iodo-2-methyl propane (0.25 mL, 2.2 mmol) followed by potassium carbonate (2.7 g, 20 mmol). The resulting mixture was stirred at room temperature for 2 days. The mixture was then diluted with water and extracted with EtOAc. The combined organic extracts were washed with brine, dried and evaporated under reduced pressure to afford a crude product, which was purified by flash chromatography on silica gel (*n*-hexane/EtOAc 5:1) to give **2** (220 mg, 25% yield) as pure yellow oil. ^{1}H-NMR ($CDCl_3$) δ: 0.85 (t, *J*=6.4 Hz, 6H); 0.93 (d, *J*=6.6 Hz, 3H); 1.08 (d, *J*=6.6 Hz, 3H); 1.27 (s, 9H); 2.02-2.19 (m, 2H); 3.02-3.13 (m, 1H); 3.24-3.34 (m, 1H); 4.05 (d, *J*=10.6 Hz, 1H); 7.40-7.52 (m, 3H); 7.56-7.59 (m, 2H); 7.65-7.69 (m, 2H); 7.90-7.94 (m, 2H).

(*R*)-2-(*N*-isobutylbiphenyl-4-ylsulfonamido)-3-methylbutanoic acid (3). TFA (2.1 mL, 27.4 mmol) was added dropwise to a stirred, ice-chilled solution of *tert*-butyl ester **2** (217 mg, 0.48 mmol) in freshly distilled dichloromethane (3.8 mL). The mixture was stirred under these reaction conditions for 5h and the solvent was removed *in vacuo.* Yellow oil, 179 mg, 95% yield. ^{1}H-NMR ($CDCl_3$) δ: 0.78 (d, *J*=6.6 Hz, 3H); 0.85 (d, *J*=6.6 Hz, 6H); 0.92 (d, *J*=6.6 Hz, 3H); 1.93-2.18 (m, 2H); 2.94-3.05 (m, 1H); 3.19-3.30 (m, 1H); 4.03 (d, *J*=10.8 Hz, 1H); 7.40-7.53 (m, 3H); 7.58-7.61 (m, 2H); 7.66-7.70 (m, 2H); 7.88-7.92 (m, 2H).

(*R*)-*N*-hydroxy-2-(*N*-isobutylbiphenyl-4-ylsulfonamido)-3-methylbutanamide (EN204). 1-[3-(Dimethylamino)propyl]-3-ethyl carbodiimide hydrochloride (EDC) was added portionwise

(118 mg, 0.61 mmol) to a stirred and cooled solution (0 ºC) of the carboxylic acid **3** (160 mg, 0.41 mmol), and *O*-(*tert*-butyldimethylsilyl)hydroxylamine (91 mg, 0.61 mmol) in freshly distilled CH_2Cl_2 (20 mL). After stirring at room temperature overnight, the mixture was washed with water and the organic phase was dried and evaporated *in vacuo*. *O*-silylate intermediate was purified by flash chromatography (*n*-hexane/EtOAc 6:1) to give a yellow oil (68 mg, 32% yield). TFA (0.5 mL, 6.5 mmol) was added dropwise to a stirred and ice-chilled solution of *O*-silylate (60 mg, 0.11 mmol) in CH_2Cl_2 (1.0 mL). The solution was stirred under these reaction conditions for 5h and the solvent was removed *in vacuo*. Hydroxamic acid **EN204** was obtained after trituration with *n*-hexane and Et_2O as a white solid (22 mg, 50% yield). ^{1}H-NMR ($CDCl_3$) δ: 0.36 (d, *J*=6.6 Hz, 3H); 0.85-0.93 (m, 9H); 2.02-2.34 (m, 2H); 2.93-3.03 (m, 1H); 3.24-3.36 (m, 1H); 3.63 (d, *J*=10.9 Hz, 1H); 7.42-7.52 (m, 3H); 7.59-7.63 (m, 2H); 7.71-7.75 (m, 2H); 7.84-7.88 (m, 2H); 9.42 (br s, 1H).

3-(Biphenyl-4-ylsulfonamido)propanoic acid (4). Biphenyl-4-sulfonyl chloride (1.56 g, 6.17 mmol) was added to a solution of 3-aminopropanoic acid (500 mg, 5.61 mmol) in H_2O (3.3 mL) and dioxane (3.3 mL) containing Et_3N (1.17 mL, 8.4 mmol). The mixture was stirred at room temperature overnight, the dioxane was evaporated and the residue was treated with EtOAc and washed with HCl 1N and brine. Organic layers were then collected, dried over Na_2SO_4, and evaporated *in vacuo*. The crude product was triturated with *n*-hexane to yield carboxylate **4** as a white solid (1.16 g, 70% yield). Mp: 138-140°C; ^{1}H-NMR [$(CD_3)_2$co] δ: 2.57 (t, *J*=6.7 Hz, 2H); 3.18-3.27 (m, 2H); 6.60 (t, *J*=5.4 Hz, 1H); 7.44-7.57 (m, 3H); 7.68-7.78 (m, 2H); 7.87-8.00 (m, 4H).

3-(Biphenyl-4-ylsulfonamido)-*N*-(tert-butyldimethylsilyloxy)propanamide (5). 1-[3-(Dimethylamino)propyl]-3-ethyl carbodiimide hydrochloride (EDC) was added portionwise (188 mg, 0.98 mmol) to a stirred and cooled solution (0 ºC) of the carboxylic acid **4** (200 mg, 0.65 mmol), and *O*-(*tert*-butyldimethylsilyl)hydroxylamine (144 mg, 0.98 mmol) in freshly

distilled CH_2Cl_2 (14 mL). After stirring at room temperature overnight, the mixture was washed with water and the organic phase was dried and evaporated *in vacuo*. *O*-silylate intermediate was purified by flash chromatography (*n*-hexane/EtOAc 2:1) to give a yellow oil (68 mg, 24% yield). ^{1}H-NMR ($CDCl_3$) δ: 0.17 (s, 6H); 0.94 (s, 9H); 2.30-2.45 (m, 2H); 3.22-3.31 (m, 2H); 5.50 (brs, 1H); 7.40-7.51 (m, 3H); 7.57-7.61 (m, 2H); 7.69-7.73 (m, 2H); 7.90-7.94 (m, 2H).

3-(Biphenyl-4-ylsulfonamido)-*N*-hydroxypropanamide (FO9). TFA (0.7 mL, 8.9 mmol) was added dropwise to a stirred and ice-chilled solution of *O*-silylate **5** (68 mg, 0.16 mmol) in CH_2Cl_2 (4.5 mL). The solution was stirred under these reaction conditions for 5h and the solvent was removed *in vacuo*. Hydroxamic acid **FO9** was obtained after trituration with Et_2O as a white solid (25 mg, 50% yield). Mp: 142-144°C; ^{1}H-NMR [$(CD_3)_2CO$] δ: 2.34 (t, *J*=6.4, 2H); 3.18-3.21 (m, 2H); 6.62 (m, 1H); 7.43-7.56 (m, 3H); 7.72-7.76 (m, 2H); 7.85-7.97 (m, 4H); 10.02 (s, 1H).

***tert*-Butyl 2-(2-(4-hydroxyphenylthio)phenyl)acetate (7).** A solution of carboxylic acid **6** (1.3 g, 5.2 mmol) in toluene (10 mL) containing *N*,*N*-dimethylformamide di-*tert*-butyl acetal (5 mL, 20.8 mmol) was heated to 95ºC for 3 h. The solvent was then evaporated and the crude product was purified by flash chromatography on silica gel (*n*-hexane/AcOEt = 6:1) to give **7** (1.0 g, 61 %) as yellow oil. ^{1}H-NMR ($CDCl_3$) δ: 1.47 (s, 9H); 3.66 (s, 2H); 5.27 (s, 1H); 6.74-6.78 (m, 2H); 7.12-7.27 (m, 6H).

***tert*-Butyl 2-(2-(4-(3-(1,3-dioxoisoindolin-2-yl)propoxy)phenylthio)phenyl)acetate (8).** A mixture of phenol **7** (1.0 g, 3.1 mmol) and K_2CO_3 (436 mg, 3.2 mmol) in dry acetone (3 mL) was stirred for 3 h at room temperature. 2-(3-Bromopropyl)isoindoline-1,3-dione (1.0 g, 3.79 mmol) in acetone (1 mL) was then added. The mixture was then refluxed for 16 h with constant stirring under nitrogen atmosphere, and TLC analysis indicated all the starting materials had been consumed. After removal of acetone under reduced pressure, the reaction mixture was poured into water and extracted with ethyl acetate. The combined organic layer was washed

successively with hydrochloric acid, water, and brine and dried over anhydrous Na_2SO_4. After removal of solvent, the desired product **8** was obtained as a yellow oil (1.6 g, 100 %). ^{1}H-NMR ($CDCl_3$) δ: 1.44 (s, 9H); 2.11-2.24 (m, 2H); 3.73 (s, 2H); 3.90 (t, *J*=6.8 Hz, 2H); 4.01 (t, *J*=6.0 Hz, 2H), 6.72-6.76 (m, 2H); 7.10-7.26 (m, 6H); 7.69-7.88 (m, 4H).

***tert*-Butyl 2-(2-(4-(3-(1,3-dioxoisoindolin-2-yl)propoxy)phenylsulfonyl)phenyl)acetate (9).** A solution of Oxone (9.2 g, 15 mmol) in H_2O (37 mL) was added slowly to a solution of **8** (950 mg, 1.88 mmol) in THF/MeOH (3:1, 37 mL). The reaction was stirred at room temperature for 24 h and the organic solvents were evaporated under reduced pressure. The obtained suspension was diluted with H_2O and the product was extracted with EtOAc. The combined organic extracts were dried over anhydrous Na_2SO_4, filtered and evaporated under reduced pressure to afford **9** as a yellow oil (516 mg, 51% yield). ^{1}H-NMR ($CDCl_3$) δ: 1.39 (s, 9H); 2.15-2.25 (m, 2H); 3.85-3.91 (m, 4H); 4.04 (t, *J*=6.0 Hz, 2H); 6.82-6.86 (m, 2H); 7.27-7.31 (m, 1H); 7.37-7.56 (m, 2H); 7.69-7.87 (m, 6H); 8.03-8.08 (m, 1H).

2-(2-(4-(3-(1,3-Dioxoisoindolin-2-yl)propoxy)phenylsulfonyl)phenyl)acetic acid (10). TFA (4.2 mL, 54.7 mmol) was added dropwise to a stirred and ice-chilled solution of ester **9** (516 mg, 0.96 mmol) in CH_2Cl_2 (5 mL). The solution was stirred under these reaction conditions for 5h and the solvent was removed *in vacuo*. Carboxylic acid **10** was obtained after trituration with Et_2O as a white solid (350 mg, 76% yield). Mp: 168-170°C; ^{1}H-NMR ($CDCl_3$) δ: 2.10-2.21 (m, 2H); 3.92 (t, *J*=6,2 Hz, 2H); 4.00-4.06 (m, 4H); 6.74-6.81 (m, 2H); 7.31-7.36 (m, 1H); 7.45-7.63 (m, 2H); 7.67-7.83 (m, 6H); 8.25-8.30 (m, 1H).

2-(2-(4-(3-(1,3-Dioxoisoindolin-2-yl)propoxy)phenylsulfonyl)phenyl)-*N*-hydroxyacetamide (FC31). 1-[3-(Dimethylamino)propyl]-3-ethyl carbodiimide hydrochloride (EDC) was added portionwise (92 mg, 0.47 mmol) to a stirred and cooled solution (0 ºC) of the carboxylic acid **10** (153 mg, 0.31 mmol), and *O*-(*tert*-butyldimethylsilyl)hydroxylamine (47 mg, 0.31 mmol) in freshly distilled CH_2Cl_2 (8 mL). After

stirring at room temperature overnight, the mixture was washed with water and the organic phase was dried and evaporated *in vacuo*. *O*-silylate intermediate was used in the next step without further purification (163 mg, 84% yield). ^{1}H-NMR ($CDCl_3$) δ: 0.12 (s, 6H); 0.91 (s, 9H); 2.17-2.26 (m, 2H); 3.70 (s, 2H); 3.90(t, *J*=6.4 Hz, 2H); 4.07 (t, *J*=5.6 Hz, 2H); 6.87-6.91 (m, 2H); 7.36-7.95 (m, 10H); 9.16 (s, 1H). TFA (1.2 mL, 15.3 mmol) was added dropwise to a stirred and ice-chilled solution of *O*-silylate intermediate (163 mg, 0.27 mmol) in CH_2Cl_2 (2.1 mL). The solution was stirred under these reaction conditions for 5h and the solvent was removed *in vacuo*. Hydroxamic acid **FC31** was obtained after trituration with Et_2O as a white solid (121 mg, 91% yield). Mp: 154-155°C; ^{1}H-NMR ($CDCl_3$) δ: 2.13-2.25 (m, 2H); 3.80 (s, 2H); 3.89 (t, *J*=6.1 Hz, 2H); 4.07 (t, *J*=5.9 Hz, 2H); 6.84-6.89 (m, 2H); 7.43-7.53 (m, 3H); 7.69-7.85 (m, 6H); 7.96-8.00 (m, 1H).

2-(5-Bromo-*N*-isopropoxythiophene-2-sulfonamido)acetic acid (12). TFA (3.1 mL, 41 mmol) was added dropwise to a stirred and ice-chilled solution of ester **11** (300 mg, 0.72 mmol) in CH_2Cl_2 (5.7 mL). The solution was stirred under these reaction conditions for 5h and the solvent was removed *in vacuo*. Carboxylic acid **12** was obtained after trituration with *n*-hexane as a beige solid (213 mg, 83% yield). ^{1}H-NMR ($CDCl_3$) δ: 1.27 (d, *J*=6.2 Hz, 6H); 3.82 (brs, 2H); 4.57 (septet, *J*=6.2 Hz, 1H); 7.17 (d, *J*=4.0 Hz, 1H); 7.45 (d, *J*=4.0 Hz, 1H).

2-(5-Bromo-*N*-isopropoxythiophene-2-sulfonamido)-*N*-hydroxyacetamide (ML25). 1-[3-(Dimethylamino)propyl]-3-ethyl carbodiimide hydrochloride (EDC) was added portionwise (172 mg, 0.9 mmol) to a stirred and cooled solution (0 ºC) of the carboxylic acid **12** (213 mg, 0.6 mmol), and *O*-(*tert*-butyldimethylsilyl)hydroxylamine (88 mg, 0.6 mmol) in freshly distilled CH_2Cl_2 (13 mL). After stirring at room temperature overnight, the mixture was washed with water and the organic phase was dried and evaporated *in vacuo*. *O*-silylate intermediate was purified by flash chromatography (*n*-hexane/EtOAc = 6:1) using a ISOLUTE Flash Si II cartridge to give a beige solid (158 mg, 54% yield). ^{1}H-NMR ($CDCl_3$) δ: 0.20 (s, 6H); 0.97 (s,

9H); 1.27 (d, *J*=6.2 Hz, 6H); 3.71 (s, 2H); 4.47 (septet, *J*=6.2 Hz, 1H); 7.18 (d, *J*=4.0 Hz, 1H); 7.46 (d, *J*=4.0 Hz, 1H); 8.43 (brs, 1H). TFA (1.3 mL, 17.6 mmol) was added dropwise to a stirred and ice-chilled solution of *O*-silylate intermediate (153 mg, 0.31 mmol) in CH_2Cl_2 (2.5 mL). The solution was stirred under these reaction conditions for 5h and the solvent was removed *in vacuo*. Hydroxamic acid **ML25** was obtained after trituration with Et_2O as a white solid (87 mg, 74% yield). Mp: 120-121°C; ^{1}H-NMR ($CDCl_3$) δ: 1.26 (d, *J*=6.2 Hz, 6H); 3.76 (brs, 2H); 4.47 (septet, *J*=6.2 Hz, 1H); 7.18 (d, *J*=4.0 Hz, 1H); 7.46 (d, *J*=4.0 Hz, 1H); 8.97 (brs, 1H).

***N*-Isopropoxy-4-phenoxybenzamide (13).** A solution of 4-phenoxybenzoic acid (500 mg, 2.33 mmol) and EDC (490 mg, 2.5 mmol) in CH_2Cl_2 (15 mL) was added to a stirred solution of *O*-isopropyl hydroxylamine hydrochloride (285 mg, 2.5 mmol) and *N*-methylmorpholine (NMM) in freshly distilled CH_2Cl_2 (15 mL). After stirring at room temperature overnight, the mixture was washed with HCl 10%, $NaHCO_3$ solution and brine. The organic phase was dried and evaporated *in vacuo*. The crude product was purified by flash chromatography (CH_2Cl_2/MeOH 20:1) to give a yellow oil (404 mg, 64% yield). ^{1}H-NMR ($CDCl_3$) δ: 1.30 (d, *J*=6.2 Hz, 6H); 4.26 (septet, *J*=6.2 Hz, 1H); 6.97-7.06 (m, 4H); 7.13-7.21 (m, 1H); 7.34-7.42 (m, 2H); 7.69-7.75 (m, 2H); 8.45 (s, 1H).

(*R*)-*tert*-Butyl 4-(1,3-dioxoisoindolin-2-yl)-2-(*N*-isopropoxy-4-phenoxybenzamido)butanoate (15). Diisopropyl azodicarboxylate (DIAD) (0.16 mL, 0.82 mmol) was added dropwise to a solution containing (*S*)-*tert*-butyl 4-(1,3-dioxoisoindolin-2-yl)-2-hydroxybutanoate **14** (100 mg, 0.33 mmol), the amide **13** (90 mg, 0.33 mmol) and triphenylphosphine (260 mg, 0.99 mmol) in anhydrous THF (5 mL) under nitrogen atmosphere. The resulting solution was stirred for 5h at room temperature and evaporated under reduced pressure to afford a crude product which was purified by flash chromatography on silica gel (*n*-hexane/EtOAc = 3:1) to yield **15** (85 mg, 45%) as pure yellow oil. ^{1}H-NMR ($CDCl_3$) δ: 1.23-

1.30 (m, 6H); 1.43 (s, 9H); 2.21-2.32 (m, 2H); 3.95 (t, *J*=6.7 Hz, 2H); 4.22 (septet, *J*=6.2 Hz, 1H); 5.57 (t, *J*=5.3 Hz, 1H); 6.91-7.15 (m, 5H); 7.30-7.38 (m, 2H); 7.67-7.73 (m, 2H); 7.79-7.84 (m, 4H).

(*R*)-4-(1,3-Dioxoisoindolin-2-yl)-2-(*N*-isopropoxy-4-phenoxybenzamido)butanoic acid (16). TFA (0.61 mL, 7.98 mmol) was added dropwise to a stirred and ice-chilled solution of ester **15** (80 mg, 0.14 mmol) in CH_2Cl_2 (1.5 mL). The solution was stirred under these reaction conditions for 5h and the solvent was removed *in vacuo*. Carboxylic acid **16** was obtained after trituration with *n*-hexane and Et_2O as a white solid (66 mg, 94% yield). ^{1}H-NMR ($CDCl_3$) δ: 1.24 (d, *J*=5.6 Hz, 6H); 2.41 (dd, *J*=6.4 Hz, 2H); 3.94 (t, *J*=6.7 Hz, 2H); 4.23 (septet, *J*=5.6 Hz, 1H); 5.29 (m, 2H); 6.89-6.93 (m, 2H); 7.03-7.07 (m, 2H); 7.16-7.24 (m, 1H); 7.36-7.44 (m, 2H); 7.65-7.81 (m, 4H); 7.95-7.99 (m, 2H).

(*R*)-*N*-(4-(1,3-Dioxoisoindolin-2-yl)-1-(hydroxyamino)-1-oxobutan-2-yl)-4-phenoxybenzamide (EN181). 1-[3-(Dimethylamino)propyl]-3-ethyl carbodiimide hydrochloride (EDC) (36 mg, 0.19 mmol) was added portionwise to a stirred and cooled solution (0 ºC) of the carboxylic acid **16** (66 mg, 0.13 mmol), and *O*-(*tert*-butyldimethylsilyl)hydroxylamine (28 mg, 0.19 mmol) in freshly distilled CH_2Cl_2 (4 mL). After stirring at room temperature overnight, the mixture was washed with water and the organic phase was dried and evaporated *in vacuo*. *O*-silylate intermediate was purified by flash chromatography (*n*-hexane/EtOAc = 2:1) to give a yellow oil (16 mg). TFA (0.1 mL, 1.37 mmol) was added dropwise to a stirred and ice-chilled solution of *O*-silylate intermediate (15 mg, 0.024 mmol) in CH_2Cl_2 (1 mL). The solution was stirred under these reaction conditions for 5h and the solvent was removed *in vacuo*. Hydroxamic acid **EN181** was obtained after trituration with Et_2O as a white solid (8.5 mg, 77% yield). ^{1}H-NMR (acetone-d_6) δ: 2.29-2.41 (m, 2H); 2.86 (brs, 1H); 3.81-3.95 (m, 2H); 5.25 (dd, *J*=4.3 Hz, 1H); 6.93-6.98 (m, 2H); 7.10-7.14 (m, 2H); 7.22-7.29 (m, 1H); 7.44-7.52 (m, 2H); 7.74-7.80 (m, 4H); 7.96-8.01 (m, 2H); 10.33 (s, 1H).

***N*-(1-Adamantyloxy)-4-methoxybenzenesulfonamide (18).** A solution of 4-methoxybenzene-1-sulfonyl chloride (371 mg, 1.79 mmol) in anhydrous THF (5 mL) was added dropwise to a stirred and cooled (0 °C) solution of *O*-(1-adamantyl)oxyamine **17** (300 mg, 1.79 mmol) and *N*-methylmorpholine (0.2 mL, 1.79 mmol) in anhydrous THF (5 mL). After stirring at room temperature for 4 days, the reaction mixture was diluted with EtOAc and washed with H_2O. The organic phase was dried over anhydrous Na_2SO_4, filtered and evaporated under reduced pressure. The crude product was purified by flash chromatography on silica gel (*n*-hexane/EtOAc = 4:1) to yield **18** as a white solid (292 mg, 48% yield).^{1}H-NMR ($CDCl_3$) δ: 1.56 (m, 6H); 1.76 (d, 6H); 2.15 (m, 3H); 3.88 (s, 3H); 6.36 (s, 1H); 6.97-7.01 (m, 2H); 7.82-7.87 (m, 2H).

***tert*-Butyl 2-(*N*-1-adamantyloxy-4-methoxyphenylsulfonamido)acetate (19).** A solution of sulfonamide **18** (292 mg, 0.87 mmol) in anhydrous DMF (3 mL) was treated with *tert*-butyl bromoacetate (0.15 mL, 1.02 mmol), caesium carbonate (283 mg, 0.87 mmol) and tetrabutylammonium hydrogen sulfate (295 mg, 0.87 mmol). The reaction mixture was stirred for 3 days at room temperature, diluted with H_2O and extracted with EtOAc. The combined organic extracts were dried over anhydrous Na_2SO_4, filtered and evaporated under reduced pressure. The crude product was purified by flash chromatography on silica gel (*n*-hexane/EtOAc = 4:1) to yield **19** as a yellow solid (194 mg, 49% yield). ^{1}H-NMR ($CDCl_3$) δ: 1.49 (s, 9H); 1.62 (m, 6H); 1.90 (d, 6H); 2.18 (m, 3H); 3.75 (s, 2H); 3.88 (s, 3H); 6.98-7.02 (m, 2H); 7.79-7.83 (m, 2H).

2-(*N*-1-adamantyloxy-4-methoxyphenylsulfonamido)acetic acid (20). TFA (1.8 mL) was added dropwise to a stirred and ice-chilled solution of ester **19** (194 mg, 0.43 mmol) in CH_2Cl_2 (2 mL). The solution was stirred under these reaction conditions for 5h and the solvent was removed *in vacuo*. Carboxylic acid **20** was obtained after trituration with *n*-hexane and Et_2O as

a yellow solid (176 mg, 99% yield). Mp: 190-192 °C; ^{1}H-NMR ($CDCl_3$) δ: 1.63 (m, 6H); 1.88 (d, 6H); 2.2 (m, 3H); 3.80 (d, 2H); 3.89 (s, 3H); 7.01-7.05 (m, 2H); 7.80-7.85 (m, 2H).

***N*-hydroxy-2-(*N*-1-adamantyloxy-4-methoxyphenylsulfonamido)acetamide (CC30).** 1-[3-(Dimethylamino)propyl]-3-ethyl carbodiimide hydrochloride (EDC) (93 mg, 0.48 mmol) was added portionwise to a stirred and cooled solution (0 ºC) of the carboxylic acid **20** (176 mg, 0.48 mmol), and *O*-(*tert*-butyldimethylsilyl)hydroxylamine (71 mg, 0.48 mmol) in freshly distilled CH_2Cl_2 (9 mL). After stirring at room temperature overnight, the mixture was washed with water and the organic phase was dried and evaporated *in vacuo*. TFA (1.6 mL) was added dropwise to a stirred and ice-chilled solution of *O*-silylate intermediate (190 mg, 0.36 mmol) in CH_2Cl_2 (3.2 mL). The solution was stirred under these reaction conditions for 5h and the solvent was removed *in vacuo*. Hydroxamic acid **CC30** was obtained after trituration with Et_2O as a white solid (91 mg, 62% yield). ^{1}H-NMR (DMSO-d_6) δ: 1.55 (m, 6H); 1.81 (m, 6H); 2.11 (m, 3H); 3.79 (d, 2H); 3.87 (s, 3H); 7.15-7.20 (m, 2H); 7.76-7.79 (m, 2H); 10.6 (s, 1H).

5.2 Experimental binding studies

5.2.1 Thermolysin and pseudolysin

Three times crystallized thermolysin (activity > 7000 units/mg) was from Calbiochem. Some pseudolysin was obtained as a gift from Prof. Efrat Kessler, Tel Aviv University Sackler, Israel, and in addition obtained from Calbiochem. DMSO was from Merck. The fluorogenic substrate AGLA was obtained from Bachem, while the fluorogenic substrate BLS was from AnaSpec (ID: 929-ZN-10).

IC_{50} values of the compounds were measured both for thermolysin and pseudolysin using the two fluorogenic substrates, AGLA and BLS. The IC_{50} values for pseudolysin with the AGLA substrate were measured with the use of spectrofluorometer (Perkin Elmer

Luminiscence spectrometer LS50B), while the other IC_{50} values were measured with the 96-plate readers (Molecular Devices models Gemini XS and Spectra MAX Gemini EM).

5.2.1.1 Instrument and instrument settings. To determine the IC_{50} value for the potential inhibitors, initial rate measurements were performed at 25 °C with the different instruments and substrates. The instruments and their settings were as follows:

AGLA: These experiments were performed on either a Perkin Elmer LS 50 Luminescence spectrometer controlled by the FL WinLab Software Package (Perkin Elmer) or a Spectra Max Gemini EM Plate Reader controlled by the computer program Soft Max Pro version 4.3 (Molecular Devices). All assays were performed with an excitation wavelength of 330 nm and an emission wavelength of 460 nm, using slit widths of 10 nm.

BLS: Spectra Max Gemini EM Plate Reader controlled by the computer program Soft Max Pro version 4.3 (Molecular Devices) or a Spectra Max Gemini XS (03148, Molecular Devices). All assays were performed with an excitation wavelength of 328 nm and an emission wavelength of 393 nm.

5.2.1.2 Determination of IC_{50} values using the AGLA substrate. All the potential inhibitors were dissolved in 100% DMSO and were further diluted with water to give a concentration of 100 µM. The enzyme inhibition studies were performed under a set of different conditions which varied with substrate and enzyme used as described in the following paragraphs.

Pseudolysin: The AGLA substrate was dissolved in 50% acetic acid, giving a concentration of 500 µM. 4 µl of 1.0 µM enzyme was preincubated for 15 minutes at 25 °C with 4 µl of inhibitors (appropriate concentrations) and 100 µl of 0.1 M Tris-HCl, 5 mM $CaCl_2$, pH 8.25 and 88 µl water (Milli-Q). In the controls, inhibitor was substituted with buffer and in the inhibitor and control experiments the final DMSO concentration was less than 5 %. The enzyme reaction was

started by adding 4 µl of AGLA to the enzyme-inhibition mixture which resulted in a total reaction volume of 200 µl, with final substrate and enzyme concentrations of 10 µM and 20 nM, respectively, and a pH of 7.8. The initial reaction rate was monitored for 1 minute. Plots of v_i/v_0 against [I] were used to determine the IC_{50} value where v_i and v_0 represents the initial rate activity in the presence and absence of inhibitor, respectively. The enzyme kinetic program in Graph Pad Prism 5 was used to determine the IC_{50} value, using equation (1):

$v_i/v_0 = 1/(1+ [I] / IC_{50})$ (Eqn. 1) [35]

All experiments were performed in duplicate.

Thermolysin: A stock solution of 2.0 mM AGLA in 100% DMSO was further diluted to 75 µM in 0.1 M Hepes, pH 7.3, containing 10 mM $CaCl_2$, 0.005% Brij-35. Five µl of enzyme solution (4.4 nM) was pre-incubated for 15 minutes at 37 °C with 10 µl of inhibitors (appropriate concentrations) and 65 µl of 0.1 M Hepes, 10 mM $CaCl_2$, 0.005% Brij-35, pH 7.3. In the controls, the inhibitor was exchanged with buffer. In the inhibitor and control experiments the final DMSO concentration was 5 %. The enzyme reaction was started by adding 20 µl of AGLA (75 µM) to the enzyme-inhibition mixture which resulted in a total reaction volume of 100 µl with final substrate and enzyme concentrations of 15 µM and 0.21 nM respectively, and a pH of 7.3. The final inhibitor concentrations in the assays varied from 10^{-3} to 10^{-10} M. The initial rate reaction was followed for 30 minutes at 37 °C. The enzyme kinetic program in Sigma-Plot was used to determine the IC_{50} value and due to the large range of inhibitor concentration, the logarithm of [I] and IC_{50} was used in equation (1) which then results in equation (2):

$$\frac{vi}{v0} = \frac{1}{(1+ 10^{(pIC50-pI)})} \quad \text{(Eqn. 2)}$$

Where pI = - log [Inhibitor] in M, pIC_{50} = - log IC_{50}, All experiments were performed at least in triplicate.

5.2.1.3. Determination of IC_{50} values using the BLS substrate. The IC_{50} values of the compounds were measured both for thermolysin and pseudolysin using BLS. Thermolysin; assay buffer consisted of 0.1 M Hepes pH 7.5, 10 mM $CaCl_2$ and 0.005 % Brij-35, [substrate] = 3.33 μM, [Thermolysin] = 5 nM. Pseudolysin; assay buffer consisted of 0.1 M Hepes pH 7.5, 10 mM $CaCl_2$, 150 mM NaCl and 0.005 % Brij-35, [substrate] = 1.73 μM, [Pseudolysin] = 5 nM. The substrate-powder was dissolved in DMSO, and diluted sequential two times in assay buffer, so the fixed DMSO contribution with substrate in the assay was 1 % in the thermolysin assay and approximately 0.5 % in the Pseudolysin assay. The inhibitors were dissolved in DMSO to a stock concentration of 10 mM, and seven inhibitor concentrations were used for each inhibitor ranging from low (typical 0.1-1) to high (500) μM. The DMSO contribution was at most 5 %, but was often kept below than 1 %. Thermolysin remained unaffected by 6 % DMSO in our experiments, and therefore the varied DMSO amounts should not affect the outcome. The inhibitors were pre-incubated with enzyme for 1 hour in 96-well microtiter plates at room temperature. The enzymatic reaction was started by adding the substrate and the initial rate was followed over a period of 15 minutes. Three parallels were performed for control, where the inhibitor was replaced with buffer. The decrease in rate, due to added inhibitor, was calculated as percentage (%) relative to the controls (Softmax Pro 4.7.1), and analysed with a non-linear curve fitting (Origin 6.0) using equation (1).

5.2.1.4 Kinetic parameters. Prior to determination of the IC_{50} values, it was necessary to determine the K_m values for the two enzymes with AGLA and BLS. Each K_M determination was performed on the Perkin Elmer LS 50 Luminescence spectrometer at 25 °C with AGLA and 37 °C with BLS, using the instrument settings described above for respective substrate. Initial rates were determined with AGLA concentrations ranging from 30 - 400 μM. All assays

were performed in 0.1 M Hepes, 10 mM $CaCl_2$, 0.005 % Brij-35, pH 7.3 with AGLA and pH 7.5 with BLS, using a final concentration of 2.2 nM thermolysin and 5.0 nM pseudolysin. In the case of BLS, initial rates were determined with substrate concentrations ranging from 1.3 to 10.0 μM, higher substrate concentrations resulted in quenching. For all tests, at least two independent experiments were performed to obtain reliable K_m values. These were calculated from non-linear regression of the Michaelis-Menten equation using the Enzyme kinetic module in Sigma Plot.

5.2.2 MMPs and ADAM-17 inhibition assays

Recombinant human proMMP-2, proMMP-9 and ADAM-17 (PF133) were purchased from Calbiochem. Proenzymes were activated immediately prior to use with *p*-aminophenylmercuric acetate (APMA 2 mM for 1 h at 37 °C for MMP-2, 1 mM for 1 h at 37 °C for MMP-9). For assay measurements, the inhibitor stock solutions (10 mM in DMSO) were further diluted, at 7 different concentrations (0.01 nM-300 μM) for each MMP in the fluorimetric assay buffer (FAB: 50 mM Tris, pH = 7.5, 150 mM NaCl, 10 mM $CaCl_2$ 10, 0.05 % Brij 35 and 1 % DMSO). Activated enzyme (final concentration 0.5 nM for MMP-2, 1.3 nM for MMP-9 and 5 nM for ADAM-17) and inhibitor solutions were incubated in the assay buffer for 2 h at 25 °C. ADAM-17 was incubated for 30 min at 37 °C in another buffer at pH = 9 (Tris 25 mM, $ZnCl_2$ 25 μM, Brij-35 0.005%). After the addition of 200 μM of the fluorogenic substrate FS-6 (Bachem) in DMSO (final substrate concentration 2 μM), the hydrolysis was monitored every 10 sec for 15 min recording the increase in fluorescence (λ_{ex} = 325 nm, λ_{em} = 395 nm) using a Molecular Devices SpectraMax Gemini XS plate reader. The assays were performed in triplicate in a total volume of 200 μL per well in 96-well microtiter plates (Corning, black, NBS). The enzyme inhibition activity was expressed in relative fluorescent units (RFU). Percent of inhibition was calculated from control reactions without the inhibitor. IC_{50} was

determined using the formula: $v_i/v_o = 1/(1 + [I]/ IC_{50})$, where v_i is the initial velocity of substrate cleavage in the presence of the inhibitor at concentration [I] and v_o is the initial velocity in the absence of the inhibitor. Results were analysed using SoftMax Pro software (SoftMax Pro 4.7.1 by Molecular Devices) and GraFit software (GraFit version 4 by Erithecus Software).

5.3 Molecular modelling

5.3.1 Docking

The Internal coordinate mechanics (ICM) program [29] was used for docking the compounds into pseudolysin, thermolysin, MMP-2 and MMP-9. The inhibitors were also docked into thermolysin using the Glide program of the Schrødinger program package [30].

5.3.1.1 ICM. Enzyme – inhibitor complexes of pseudolysin (PDB-code: 1u4g), thermolysin (PDB-code: 1pe5). MMP-2 (PDB-code: 1hov), and MMP-9 (PDB-code: 1gkc) were obtained from the PDB database. The MMP-2 complex used for docking was 1hov. The MMP-2 structure in the 1hov complex has a short peptide linker replacing the internal fibronectin-domain, but is still active. This structure has been complexed with hydroxamic acid inhibitor (SC-74020) and was therefore used for docking. Crystallographic water molecules and co-crystallized small molecule inhibitors were removed and hydrogen atoms were added and optimized using the ECEPP/3 force field of ICM. The inhibitors were built using ICM and minimized before docking. A grid map that included the active site amino acids was calculated, and semi-flexible docking with flexible ligands was performed.

5.3.1.2 Glide. The molecules were drawn, hydrogen atoms were added, and the structures were energy optimized. Ligprep was used to generate tautomeric and ionic forms at pH 7.0 +/- 2.0, using Ionizer or Epik (including and excluding metal binding states) with default settings. The

thermolysin structure was pre-processed with default settings, except that all water molecules more than 1 Å from the structure were removed. Het-states was generated (with metal mode), and the selected structure was minimized with an RMSD threshold of 0.30 Å relative to the starting structure (force field OPLS 2005). The inhibitor molecule was manually deleted before a 30 Å grid was generated centroid of the co-crystallised ligand. Ligand docking was conducted using both standard precision (SP) and extra precision (EP), with the different multiple ionic and tautomeric states produced with Ionizer or epik, respectively.

5.3.2 Molecular dynamics simulation of pseudolysin-ligand interactions

The complexes after docking into pseudolysin were used as starting structures for MD simulations of pseudolysin-ligand interactions using Amber 9.0. The simulations were performed for 24 ns, and the trajectories sampled during 20-24 ns were used for calculation of an average pseudolysin-ligand structure using the ptraj package of the AMBER suite of programs.

5.3.2.1 Atomic point charges. The electrostatic potentials of each inhibitor were calculated using the antechamber program of the AMBER SUITE and the inbuilt AMI-BCC charges were used to derive atomic restrained electrostatic point (RESP) charges of the inhibitors [36-39].

5.3.2.2 Molecular dynamics simulations. A non-bonded approached was used for the metal ions [40, 41]. Zinc was assigned a formal charge of +2.0, van der Waal's radius 0.69Å and well depth ε = 0.014 kcal/mol. Calcium was assigned a formal charge of +2.0, van der Waal's radius 1.6Å and well depth ε = 0.1 kcal/mol [41]. The coordination of zinc and calcium ions in the pseudolysin structure was described by non-bonded energy terms in the calculations [41]. Zinc ions were assigned a formal charge of +2.0, van der Waals' radius 0.69Å and well depth ε =

0.014 kcal/mol. Calcium ions were assigned a formal charge of +2.0, van der Waals' radius 1.6Å and well depth ε = 0.1 kcal/mol [41]. All minimizations and MD simulations were performed with the AMBER 9.0 package [31] and a TIP3P water model. The AMBER 2003 force field was used for both ligand bound and free states of pseudolysin. All molecular systems (bound and free states) were solvated with a cubic box of water molecules and neutralized by counter ions [42]. The Particle Mesh Ewald (PME) method was used for treatment of long range electrostatic interactions [43]. The non-bonded cut off radius was 10.0 Å, and the SHAKE option [44] was used to constrain bonds involving hydrogen atoms. The dielectric constant was 1, and all molecular systems were initially minimized by the conjugate gradient method and equilibrated for 200 ps of MD. During the equilibration, the temperature was gradually increased to 300 K and kept constant post equilibration. The MD simulations were run for a total of 24 ns. The time step during MD was 2 fs, and the non-bonded pair list was updated every 25 steps. Due to the +2 charge of the zinc ion and several surrounding anionic residues, the zinc atom and its ligated amino acids needed special treatment during MD in order to prevent distortion of the active site and the zinc coordination. Two histidines, a glutamic acid and a water molecule coordinate the zinc ion in the active site. Inhibitors usually replace this water molecule with a carboxylate, hydroxamate or phosphoramidate group as observed in the x-ray structure thermolysin-inhibitor complexes. Harmonic restraining force of 50 kcal/Å and distance restraints of 2.1Å-2.5Å was therefore used between the coordinating atoms of the hydroxamate and the zinc ion. Further, harmonic restraining force (50 kcal/Å) and a distance restraint (2.10Å) were applied between zinc and its amino acid ligands: His 140 (atom NE2); His 144 (atom NE2) and Glu 164 (atom OE1). Similar approaches have also previously been used for calculations of zinc containing proteins [45, 46].

6.0 Acknowledgement

We are grateful to Prof. Efrat Kessler, Tel Aviv University Sackler, Faculty of Medicine Goldschleger Eye Research Institute, Sheba Medical Center, Tel-Hashomer 52621, Israel for contributing with pseudolysin. The project was supported by computer time from NOTUR - The Norwegian metacentre for computer time. This study was supported by fundings from the Italian Ministry of Education, University and Research (MIUR, PRIN 2007, 2007JERJPC_005) and from the University of Pisa (Fondi di Ateneo 2009, to A. R.).

Table 1. Inhibition data[a] of hydroxamates against thermolysin, pseudolysin (using two different subtrates), MMP-2, MMP-9 and ADAM-17.

Compound	IC_{50} (μM)						
	Thermolysin		Pseudolysin		MMP-2	MMP-9	ADAM-17
	BLS	AGLA	BLS	AGLA			
ARP101	800	416	798	57	0.0008 [26]	0.0067 [26]	14
EN178	NT	NT	NT	103	0.029 [22]	0.0072 [22]	1.1
EN204	608	243	226	29	0.003	0.0053	NT
FO9	30	30	79	30	2.4	26	NT
FC19	146	NT	29	17	0.23 [24]	0.098 [24]	67
FC31	132	NT	38	7	>10	>10	150
EN181	NT	NT	NT	16	9.0	8.2	9.5
ML25	29	29	31	3.3	1.1	6.2	114
LM2	9.5	NT	1.9	1.1	34 [23]	81 [23]	100
CC30	438	90	142	51	2.0	2.0	NT

[a] The IC_{50} values are the average of at least two determinations with a standard deviation of <10%. NT: not tested.

Table 2. Amino acids within 4 Å of the ligand in the average complexes from the trajectories between 20 and 24 ns of MD.

Compound	Amino acids within 4 Å of the compound
ARP101	N112, Y114, W115, H140, E141, H144, L153, I154, Y155, G160, N163, E164, L197, R198, D221, V222, H223
FO9	A113, Y114, W115, M120,V137, H140, E141, H144, Y155, E164,I190,L197, V222, H223
LM2	N112, A113, Y114, W115, H140, H144, Y155, E164, L197, R198; D206, S209, H223, H224
CC30	Y114, W115, D116, H140, E141, H144,Y155, N163, E164, V222, H223
EN178	Y114, W115, D116, G117, H140, E141, H144, Y155, E164
EN204	E111, N112, A113, T114, F129, L132, V137, H140, E141, E164, I186, L197, R198, D206, H223, H224
FC31	N112, Y114, W115, D116, G117, H140, E141, H144, Y155, E164, D221, V222, H223
FC19	N112, A113, Y114, W115, H140, E141, H144, Y155, E164, H223
EN181	N112, A113, Y114, D116, E141, H144, E148, Y155, G160, N163, E164, V222, H223.
ML25	N112, A113, Y114, F129, V137, H140, E141, H144, E164, I186, G187, I190, L197, R198, R208

Figure legends

Figure 1. General structure of the hydroxamates used for this study.

Figure 2. ARP101, FO9 and LM2 docked into the active sites of pseudolysin (PLN) and thermolysin (TLN). The ligand structure, the most important amino acids for binding and the active site zinc are shown. Colour coding of atoms; oxygen: red, nitrogen: blue, grey: carbon atoms in PLN and TLN, yellow: carbon atoms in the ligands, cyan: zinc. The directions for the subpockets are indicated for the complexes with LM2.

Figure 3. ARP101, FO9 and LM2 docked into the active sites of MMP-9. The ligand structure, the most important amino acids for binding and the active site zinc are shown. Colour coding of atoms; oxygen: red, nitrogen: blue, grey: carbon atoms in MMP-9, yellow: carbon atoms in the ligands, cyan: zinc. The directions for the subpockets are indicated for the complex with LM2.

References

[1] B.E. Turk, Discovery and development of anthrax lethal factor metalloproteinase inhibitors, Curr. Pharmaceutical Biotech. 9 (2008) 24-33.
[2] B.W. Matthews, P.M. Colman, J.N. Jansonius, K. Titani, K.A. Walsh, H. Neurath, Structure of Thermolysin, Nature New Biology 238 (1972) 41-43.
[3] B.W. Matthews, L.H. Weaver, W.R. Kester, The conformation of thermolysin, J. Biol. Chem. 249 (1974) 8030-8044.
[4] O.A. Adekoya, I. Sylte, The thermolysin family (M4) of enzymes: therapeutic and biotechnological potential, Chem. Biol. Drug. Des. 73 (2009) 7-16.
[5] B. Altincicek, M. Linder, D. Linder, K.T. Preissner, A. Vilcinskas, Microbial metalloproteinases mediate sensing of invading pathogens and activate innate immune responses in the lepidopteran model host Galleria mellonella, Infection and Immunity 75 (2007) 175-183.
[6] C.Y. Hung, K.R. Seshan, J.J. Yu, R. Schaller, J. Xue, V. Basrur, M.J. Gardner, G.T. Cole, A metalloproteinase of Coccidioides posadasii contributes to evasion of host detection, Infection and Immunity 73 (2005) 6689-6703.
[7] F. Jin, O. Matsushita, S. Katayama, S. Jin, C. Matsushita, J. Minami, A. Okabe, Purification, characterization, and primary structure of Clostridium perfringens lambda-toxin, a thermolysin-like metalloprotease, Infection and Immunity 64 (1996) 230-237.
[8] S. Miyoshi, H. Nakazawa, K. Kawata, K. Tomochika, K. Tobe, S. Shinoda, Characterization of the hemorrhagic reaction caused by Vibrio vulnificus metalloprotease, a member of the thermolysin family, Infection and Immunity 66 (1998) 4851-4855.
[9] A. Vilcinskas, M. Wedde, Insect inhibitors of metalloproteinases, IUBMB life 54 (2002) 339-343.
[10] M.A. Holmes, B.W. Matthews, Structure of thermolysin refined at 1.6 A resolution, J. Mol. Biol. 160 (1982) 623-639.
[11] B.P. Roques, Zinc metallopeptidases: active site structure and design of selective and mixed inhibitors: new approaches in the search for analgesics and anti-hypertensives, Biochemical Society transactions, 21 (Pt 3) (1993) 678-685.
[12] M.T. Khan, K. Dedachi, T. Matsui, N. Kurita, M. Borgatti, R. Gambari, I. Sylte, Dipeptide inhibitors of thermolysin and angiotensin I-converting enzyme, Curr. Topics in Med. Chem. 12 (2012) 1748-1762.
[13] M.T. Khan, O.M. Fuskevag, I. Sylte, Discovery of potent thermolysin inhibitors using structure based virtual screening and binding assays, J. Med. Chem. 52 (2009) 48-61.
[14] M.T. Khan, R. Khan, Y. Wuxiuer, M. Arfan, M. Ahmed, I. Sylte, Identification of novel quinazolin-4(3H)-ones as inhibitors of thermolysin, the prototype of the M4 family of proteinases, Bioorg. & Med. Chem. 18 (2010) 4317-4327.
[15] L. Carson, G.R. Cathcart, H. Ceri, B. Walker, B.F. Gilmore, Comparison of the binding specificity of two bacterial metalloproteases, LasB of Pseudomonas aeruginosa and ZapA of Proteus mirabilis, using N-alpha mercaptoamide template-based inhibitor analogues, Biochem. Biophys. Res. Comm. 422 (2012) 316-320.
[16] G.R. Cathcart, D. Quinn, B. Greer, P. Harriott, J.F. Lynas, B.F. Gilmore, B. Walker, Novel inhibitors of the Pseudomonas aeruginosa virulence factor LasB: a potential therapeutic approach for the attenuation of virulence mechanisms in pseudomonal infection, Antimicrobial Agents and Chemotherapy 55 (2011) 2670-2678.
[17] C.M. Kam, N. Nishino, J.C. Powers, Inhibition of thermolysin and carboxypeptidase A by phosphoramidates, Biochem. 18 (1979) 3032-3038.

[18] N. Nishino, J.C. Powers, Design of potent reversible inhibitors for thermolysin. Peptides containing zinc coordinating ligands and their use in affinity chromatography, Biochem. 18 (1979) 4340-4347.
[19] N. Nishino, J.C. Powers, Pseudomonas aeruginosa elastase. Development of a new substrate, inhibitors, and an affinity ligand, J. Biol. Chem. 255 (1980) 3482-3486.
[20] L. Englert, A. Biela, M. Zayed, A. Heine, D. Hangauer, G. Klebe, Displacement of disordered water molecules from hydrophobic pocket creates enthalpic signature: binding of phosphonamidate to the S(1)'-pocket of thermolysin, Biochim. et Biophys. Acta 1800 (2010) 1192-1202.
[21] A. Rossello, E. Nuti, P. Carelli, E. Orlandini, M. Macchia, S. Nencetti, M. Zandomeneghi, F. Balzano, G. Uccello Barretta, A. Albini, R. Benelli, G. Cercignani, G. Murphy, A. Balsamo, N-i-Propoxy-N-biphenylsulfonylaminobutylhydroxamic acids as potent and selective inhibitors of MMP-2 and MT1-MMP, Bioorg. & Med. Chem. letters 15 (2005) 1321-1326.
[22] E. Nuti, F. Casalini, S.I. Avramova, S. Santamaria, M. Fabbi, S. Ferrini, L. Marinelli, V. La Pietra, V. Limongelli, E. Novellino, G. Cercignani, E. Orlandini, S. Nencetti, A. Rossello, Potent arylsulfonamide inhibitors of tumor necrosis factor-alpha converting enzyme able to reduce activated leukocyte cell adhesion molecule shedding in cancer cell models, J. Med. Chem. 53 (2010) 2622-2635.
[23] E. Nuti, E. Orlandini, S. Nencetti, A. Rossello, A. Innocenti, A. Scozzafava, C.T. Supuran, Carbonic anhydrase and matrix metalloproteinase inhibitors. Inhibition of human tumor-associated isozymes IX and cytosolic isozyme I and II with sulfonylated hydroxamates, Bioorg. & Med. Chem. 15 (2007) 2298-2311.
[24] E. Nuti, L. Panelli, F. Casalini, S.I. Avramova, E. Orlandini, S. Santamaria, S. Nencetti, T. Tuccinardi, A. Martinelli, G. Cercignani, N. D'Amelio, A. Maiocchi, F. Uggeri, A. Rossello, Design, synthesis, biological evaluation, and NMR studies of a new series of arylsulfones as selective and potent matrix metalloproteinase-12 inhibitors, J. Med. Chem. 52 (2009) 6347-6361.
[25] A. Rossello, Nuti, E., Orlandini, E., Balsamo, A., Tuccinardi, T., Aryl-sulphonamidic dimers as metalloproteinase inhbitors, PCT WO2010010080, (2010).
[26] E. Nuti, F. Casalini, S.I. Avramova, S. Santamaria, G. Cercignani, L. Marinelli, V. La Pietra, E. Novellino, E. Orlandini, S. Nencetti, T. Tuccinardi, A. Martinelli, N.H. Lim, R. Visse, H. Nagase, A. Rossello, N-O-isopropyl sulfonamido-based hydroxamates: design, synthesis and biological evaluation of selective matrix metalloproteinase-13 inhibitors as potential therapeutic agents for osteoarthritis, J. Med. Chem. 52 (2009) 4757-4773.
[27] A. Rossello, E. Orlandini E. Balsamo, A. Tuccinardi, T. , Compounds having aryl-sulphonamidic structure useful as metalloprotease inhibitors, PCT WO2008113756, (2008).
[28] U. Neumann, H. Kubota, K. Frei, V. Ganu, D. Leppert, Characterization of Mca-Lys-Pro-Leu-Gly-Leu-Dpa-Ala-Arg-NH2, a fluorogenic substrate with increased specificity constants for collagenases and tumor necrosis factor converting enzyme, Analytical biochemistry 328 (2004) 166-173.
[29] R. Abagyan, T. Maxim, D. Kuznetsov, ICM-A new method for Protein Modelling and Design: Applications to Docking and Structure Prediction from the Distorted Native Conformation, J. Comput. Chem. 15 (1994) 488-506.
[30] Schrødinger Release 2014-1, Maestro, V., Schrødinger, LLC, New York, NY, 2014
[31] D.A. Case, T.E. Cheatham, 3rd, T. Darden, H. Gohlke, R. Luo, K.M. Merz, Jr., A. Onufriev, C. Simmerling, B. Wang, R.J. Woods, The Amber biomolecular simulation programs, J. Comput. Chem. 26 (2005) 1668-1688.
[32] A. Biela, N.N. Nasief, M. Betz, A. Heine, D. Hangauer, G. Klebe, Dissecting the hydrophobic effect on the molecular level: the role of water, enthalpy, and entropy in ligand binding to thermolysin, Angew. Chem. Int. Ed. Engl. 52 (2013) 1822-1828.

[33] O.A. Adekoya, S. Sjoli, Y. Wuxiuer, I. Bilto, S.M. Marques, M.A. Santos, E. Nuti, G. Cercignani, A. Rossello, J.O. Winberg, I. Sylte, Inhibition of pseudolysin and thermolysin by hydroxamate-based MMP inhibitors, Eur. J. Med. Chem. 89 (2015) 340-348.
[34] J. Travis, J. Potempa, Bacterial proteinases as targets for the development of second-generation antibiotics, Biochim. et Biophys. Acta 1477 (2000) 35-50.
[35] R.A. Copeland, Enzymes: A Practical Introduction to Structure,Mechanisms and Data analysis, Second ed., John Wiley and Sons INC, 2000.
[36] C.I. Bayly, Piotr Cieplak, W.D. Cornell, P.A. Kollman, A Well-Behaved Electrostatic Potential Based Method Using Charge Restraints for Deriving
Atomic Charges: The RESP Model, J . Phys. Chem. 97 (1993) 10269-10280.
[37] W.D. Cornell, P. Cieplak, C.I. Bayly, P.A. Kollman, Application of Resp Charges to Calculate Conformational Energies, Hydrogen-Bond Energies, and Free-Energies of Solvation, J. Am. Chem. Soc. 115 (1993) 9620-9631.
[38] A. Jakalian, B.L. Bush, D.B. Jack, C.I. Bayly, Fast, efficient generation of high-quality atomic Charges. AM1-BCC model: I. Method, J. Comput. Chem. 21 (2000) 132-146.
[39] A. Jakalian, D.B. Jack, C.I. Bayly, Fast, efficient generation of high-quality atomic charges. AM1-BCC model: II. Parameterization and validation, J. Comput. Chem. 23 (2002) 1623-1641.
[40] R.H. Stote, M. Karplus, Zinc binding in proteins and solution: a simple but accurate nonbonded representation, Proteins 23 (1995) 12-31.
[41] G.E. Terp, I.T. Christensen, F.S. Jorgensen, Structural differences of matrix metalloproteinases. Homology modeling and energy minimization of enzyme-substrate complexes, J. Biomol. Struct Dyn. 17 (2000) 933-946.
[42] J. Åqvist, Calculation of absolute binding free energies for charged ligands and effects of long-range electrostatic interactions, J. Comput. Chem. 17 (1996) 1587-1597.
[43] T. Darden, D. York, L. Pedersen, Particle mesh Ewald: An $N\cdot\log(N)$ method for Ewald sums in large systems, J. Chem. Phys. 98 (1993) 10089-10092.
[44] W.F.v. Gunsteren, H.T.C. Berendsen, Algorithms for macromolecular dynamics and contraints dynamics, Molecular Physics 34 (1977) 1311.
[45] S. Tate, A. Ohno, S.S. Seeram, K. Hiraga, K. Oda, M. Kainosho, Elucidation of the mode of interaction of thermolysin with a proteinaceous metalloproteinase inhibitor, SMPI, based on a model complex structure and a structural dynamics analysis, J. Mol. Biol. 282 (1998) 435-446.
[46] Z.R. Wasserman, C.N. Hodge, Fitting an inhibitor into the active site of thermolysin: a molecular dynamics case study, Proteins 24 (1996) 227-237.

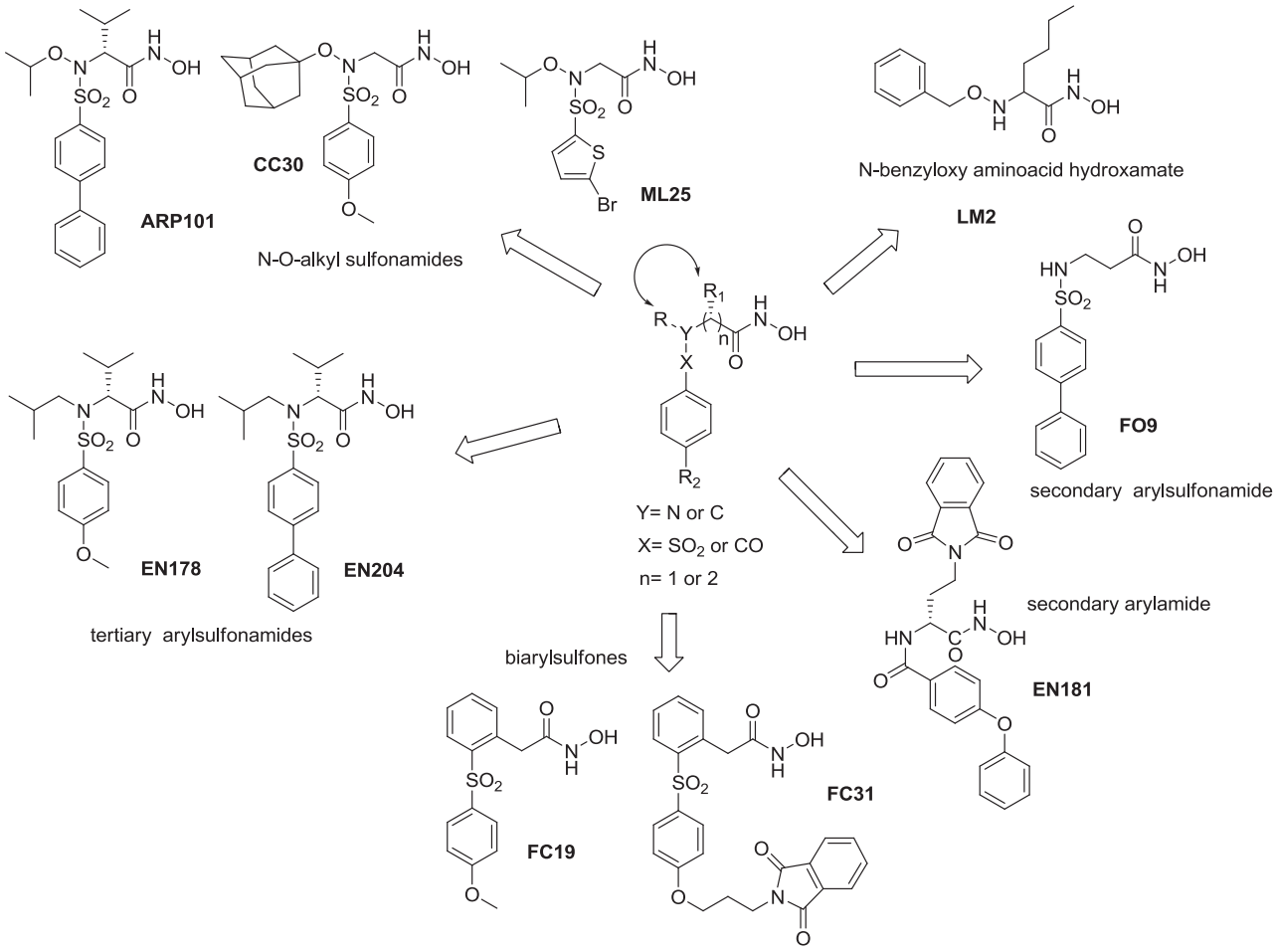
ARP101
CC30
N-O-alkyl sulfonamides
ML25
N-benzyloxy aminoacid hydroxamate
LM2
FO9
secondary arylsulfonamide
EN178
EN204
tertiary arylsulfonamides
Y= N or C
X= SO2 or CO
n= 1 or 2
secondary arylamide
EN181
biarylsulfones
FC19
FC31

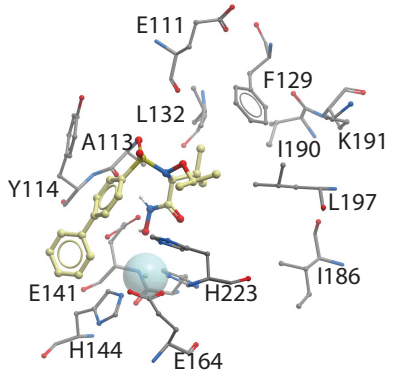

PLN - ARP101

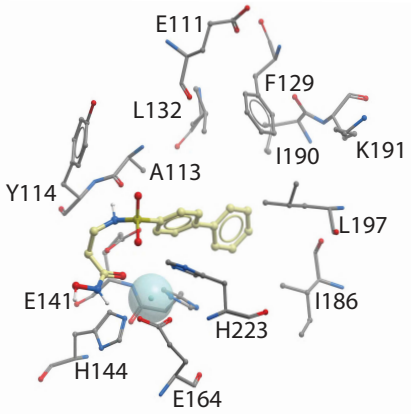

PLN - FO9

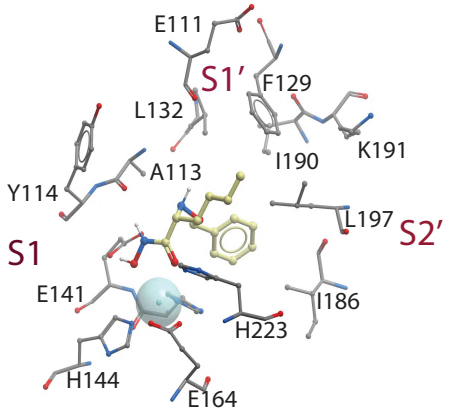

PLN - LM2

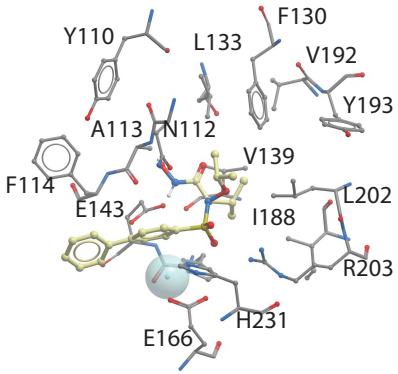

TLN - ARP101

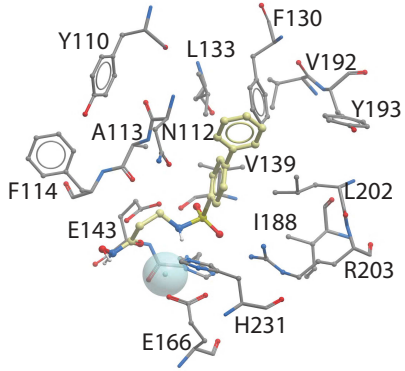

TLN - FO9

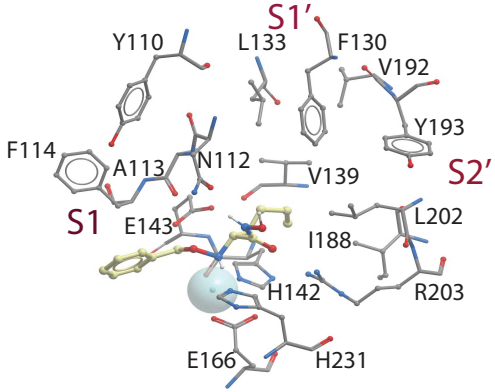

TLN - LM2

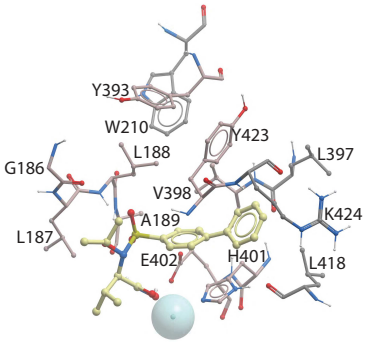

MMP-9 - ARP101

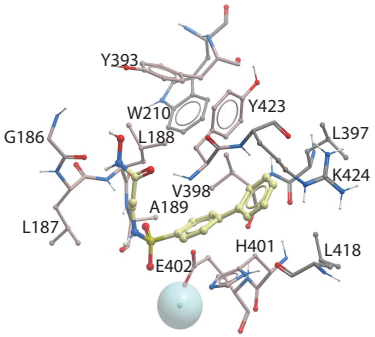

MMP-9 - FO9

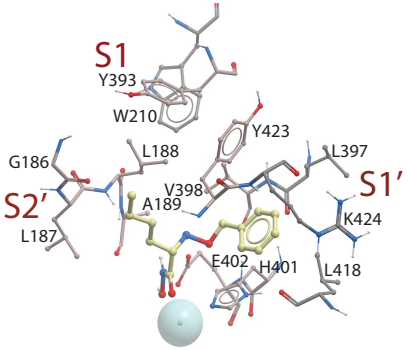

MMP-9 - LM2